NATIONAL ADVISORY COMMITTEE FOR AERONAUTICS

WARTIME REPORT

ORIGINALLY ISSUED
May 1946 as
Memorandum Report A6A09

TESTS OF A JET-MOTOR AIR-INTAKE DUCT SYSTEM ON A 1/4-SCALE STUB-WING MODEL OF A PURSUIT-TYPE AIRPLANE

By Frederick H. Hanson, Jr.

Ames Aeronautical Laboratory
Moffett Field, California

NACA

WASHINGTON

MR No. A6A09

NATIONAL ADVISORY COMMITTEE FOR AERONAUTICS

MEMORANDUM REPORT

for the

Air Technical Service Command, U. S. Army Air Forces

TESTS OF A JET-MOTOR AIR-INTAKE DUCT SYSTEM ON A 1/4-SCALE STUB-WING MODEL OF A PURSUIT-TYPE AIRPLANE

By Frederick H. Hanson, Jr.

SUMMARY

Wind-tunnel tests were made to determine the characteristics of the jet-motor air-intake duct system for a pursuit-type airplane. Modifications were made to both the external and internal design of the duct system to secure a higher critical compressibility speed and higher pressure recovery at the jet-motor air intakes.

By increasing the camber of the duct lips, the critical Mach number, as estimated from measured pressure distribution, was increased from 0.48 to 0.64 for the high-speed condition. A Mach number of 0.64, however, is below the estimated critical Mach number of the airplane for high-speed flight and it does not appear possible to secure a sufficiently high critical Mach number with the ducts in their present position and operating at an inlet-velocity ratio less than 1.0. Removing the boundary-layer air at the duct entrance resulted in a pressure recovery of $0.71q_0$ for the high-speed flight condition. Without boundary-layer removal the pressure recovery was $0.48q_0$ for the same condition. In order to secure high pressure recovery without increasing the external drag, it will be necessary to find some means of removing the boundary layer other than by a flap on the boundary-layer exit duct, which was the system used to obtain a pressure recovery of $0.71q_0$. A system using the I-40 jet-motor exhaust as a jet pump to remove the boundary layer might prove satisfactory

and at the same time not cause an increase in the external drag of the airplane.

The relative importance of pressure recovery ahead of the jet motor and external drag was evaluated for the sea-level high-speed condition. Information from jet-motor data indicated that a decrease in pressure recovery of 10 percent resulted in a change in thrust at maximum speed equivalent to an increase in drag coefficient of 0.0008. On this basis, a duct system using a streamlined bump on the boundary-layer exit duct to provide a suction pressure for boundary-layer removal was developed for which the drag increase due to the bump was more than compensated for by an increase in the pressure recovery. The flow in this system was not as desirable from the viewpoint of the minimum inlet-velocity ratio for flow stability as the system without boundary-layer control.

INTRODUCTION

With the increasing use of jet-propulsion units for modern high-performance aircraft, it has become necessary to conduct considerable research on duct systems which supply air to these units. It is desirable that duct systems have the following characteristics:

1. Low external drag
2. High critical speed
3. Low pressure losses

If possible, the duct system should be located on the airplane so that it will not interfere with visibility and major structural components, or take up a great deal of space.

The importance of duct systems has been largely underrated in the past, the general practice being to sacrifice good design of the duct system to the structure and arrangement of the rest of the airplane. With the advent of the jet-propulsion unit, the duct system becomes of considerable importance, as it greatly influences the performance of the airplane in all conditions of flight. It is desirable, therefore, to thoroughly design and test the duct system while the airplane is still in the design stage. Neglecting to do this may seriously impair the performance of the final airplane.

This report is concerned primarily with the characteristics of a duct system designed for an I-40 jet-propulsion engine. The airplane for which the air intake ducts are designed is a high-speed pursuit-type aircraft that is powered by two different types of propulsive units: (1) a General Electric TG-100 gas turbine which drives a four-blade tractor propeller, and (2) a General Electric I-40 jet-propulsion engine which exhausts through a blast tube at the end of the fuselage. The TG-100 turbine is located in the nose of the airplane. Air for this unit is taken in through an annular opening in the cowling. The gases from the turbine are exhausted through a blast tube on the underside of the fuselage. The I-40 jet-propulsion engine is located just aft of the middle of the fuselage. Air for this unit is taken in through two partially submerged entrances on the top half of the fuselage and approximately 43 percent wing chord aft the wing leading edge. For cruising, this airplane will operate on the TG-100 unit only, while for high-speed flight the I-40 unit will provide additional thrust.

This report presents the results of the tests to determine the critical speed, pressure recovery, and incremental drag of the I-40 duct system. These tests were made in the Ames 7- by 10-foot wind tunnel.

SYMBOLS AND COEFFICIENTS

The following symbols and coefficients are used in this report:

H	total pressure, pounds per square foot
p	local static pressure, pounds per square foot
P	pressure coefficient $\left(\frac{p - p_o}{q_o}\right)$
A/S	ratio of duct-entrance area to airplane wing area (S is 1/4-scale wing area)
V_A/V_o	duct inlet-velocity ratio
$C_{D_{int.}}$	internal drag coefficient $\left[\frac{2A}{S}\left(\frac{V_A}{V_o}\right)\left(\sqrt{\frac{(H_A - p_o)}{q_o}}\right)\right]$

$C_{D_{total}}$ total drag coefficient (Drag/$q_o S$)

$C_{D_{ext.}}$ external drag coefficient $\left(C_{D_{total}} - C_{D_{int.}}\right)$

T_c propeller thrust coefficient (Thrust/$\rho_o V_o^2 D^2$)

α angle of attack of wing, degrees

q_o free-stream dynamic pressure, pounds per square foot

Subscripts

A station at duct inlet

B station at compressor inlet

o free-stream conditions

MODEL AND APPARATUS

Views of a 1/4-scale stub-wing model of the airplane are shown in figures 1, 2, 3, and 4. The important components of the model are shown in figure 1 and important model dimensions are given in table I. The wing section of the airplane is a modified NACA 65(112)-213 airfoil, ordinates for which are given in table II. A side view of the model with the original ducts is shown in figure 2. The original ducts are shown separately in figure 3.

The model was powered with a General Electric two-pole motor rated at 150 horsepower at 5000 rpm. The propeller used was of Aeroproducts H-20-156-12i3 blade form, 3.00 feet in diameter. The model mounted in the tunnel with the propeller on is shown in figure 4. The configuration when the fuselage is without ducts, as shown in figure 4, is designated as the basic fuselage configuration. Air was taken from the I-40 plenum chamber through the right wing, passed through a mercury seal, and finally through a centrifugal pump located outside the building. A calibrated Venturi meter was used in the line to measure the flow through the duct system.

The static pressure recovery in the I-40 jet-motor plenum chamber was measured as the average of the six static tubes

shown in figure 1. These were located at the station of the motor air intakes. For boundary-layer-control tests, part of the boundary layer present at the duct entrances was exhausted out the bottom of the fuselage through the boundary-layer duct shown in figures 1 and 3.

TESTS

The external-pressure-distribution tests of the duct system were made through a range of inlet-velocity ratios from $V_A/V_O \cong 0.2$ to $V_A/V_O \cong 1.0$ at an angle of attack of 1°. The range of angles of attack from $\alpha = -2^\circ$ to $\alpha = 8^\circ$ was covered for $V_A/V_O \cong 0.6$, as this was approximately the high-speed inlet-velocity ratio. Pressure distributions were measured for the power-on condition through a range of angles of attack from $\alpha = -2^\circ$ to $\alpha = 8^\circ$ and at inlet-velocity ratios for several values of the propeller thrust coefficient.

Internal pressures and drags were measured through the angle-of-attack range ($\alpha = -2^\circ$ to 8°) at inlet-velocity ratios from $V_A/V_O = 0$ to $V_A/V_O = 1.0$ for the power-off condition. Additional tests were made at thrust coefficients and inlet-velocity ratios corresponding to those in flight for take-off and climb conditions.

All tests except those with the propeller operating were made at a tunnel dynamic pressure of 40 pounds per square foot. This corresponds to an average Reynolds number based on the model wing chord of $R \cong 4 \times 10^6$, and an average Mach number, $M \cong 0.17$. The tunnel dynamic pressures with the propellers operating ranged from 3.8 pounds per square foot for a propeller thrust coefficient of 1.57 to 34.4 pounds per square foot for a propeller thrust coefficient of 0.015.

Tunnel-wall corrections were applied only to the angle of attack, the effect of the fuselage being neglected. This correction was determined by the method of reference 1. No corrections were applied to the drag data, other than to take into account the internal drag coefficient which is described in the appendix. Only data on the incremental drag of the various components were desired, so that the standard wind-tunnel drag corrections could be neglected with very little error.

RESULTS AND DISCUSSION

External Pressure Distribution Over I-40 Air-Intake Ducts

The original I-40 jet-motor air-intake ducts for the model are shown in figures 2 and 3. The pressure distribution over these original ducts (see fig. 5 for original duct contours) is shown in figure 6 for the inboard fillet, top center line, outboard corner, and outboard fillet. The pressure distribution along the inboard corner is not shown in figure 6 as these orifices were not built into the original ducts. The pressure distribution indicated that the original duct shape was unsatisfactory, so the ducts were revised to the contours shown in figure 5. Table III presents ordinates of the top center line for this revised duct. The pressure distributions for this revision are given in figure 7. The effect of inlet-velocity ratio is shown in figures 7(a) to 7(c); the effect of angle of attack is shown in figures 7(d) and 7(e). The effect of power is shown in figure 8, and the effect of a large wing-root fillet in figure 9.

These pressure distributions indicated that the revised ducts were the best of the several revisions tested, as further revisions failed to decrease the general level of pressures. The maximum negative pressure for the original ducts was $-1.8q_0$ which corresponds to a critical Mach number of 0.48. The revised ducts for the same conditions, that is, inlet-velocity ratio and angle of attack, have a general level of pressure of $-0.7q_0$ which corresponds to a critical Mach number of 0.64, which is below the estimated critical Mach number of the airplane for high speed at all altitudes. The possibility of reaching the critical Mach number in the cruise condition should not be overlooked as the maximum negative pressure reached for an inlet-velocity ratio of 0.18 is $-1.4q_0$ which corresponds to a critical Mach number of 0.53. At sea level this Mach number is equivalent to 400 miles per hour, while at 20,000 feet altitude it is equivalent to 375 miles per hour.

The high negative pressure over the ducts was the result of two factors: (1) the increased velocity of flow over the duct lips due to their own shape, and (2) the increased velocity of flow over the ducts due to the presence of the airplane wing. The position of the I-40 air-intake ducts with respect to the wing is shown in figures 2 and 10. The pressure distribution over the basic fuselage is shown in figure 11. This pressure distribution is similar to that for the wing, showing the

basically high-velocity (or low-pressure) field in which the ducts are placed. There are two ways, then, to reduce the high pressures over the ducts: (1) design the ducts so the velocity of the air does not increase while passing over them, and (2) remove the ducts from the influence of the wing. The former may be done by designing ducts that operate at an inlet-velocity ratio of about one and that have less camber than ducts which are designed to operate at lower inlet-velocity ratios. This, of course, makes the diffuser design more difficult. No very satisfactory means of removing the ducts from the influence of the wing of the airplane has been found. The present ducts could be extended forward to the leading edge of the wing, but unless more of the duct could be submerged into the fuselage, the design would not be very satisfactory. A design with the duct system located under the fuselage of the airplane was considered but would probably prove undesirable because of the proximity of the duct inlet to the ground with the possibility of sucking dirt or water into the duct when the airplane is taking off or landing on a muddy field. Also considered was a design with the ducts located on top of the rear part of the fuselage. This was rejected too, as unsatisfactory flow conditions probably would exist since the duct would be directly aft of the canopy.

Boundary-Layer Control and Factors Affecting Total-Head Profiles at Duct Entrance

In addition to causing high negative pressures over the I-40 jet-motor air-intake ducts, the wing helped to produce a thick boundary layer at the duct entrance. This was a direct result of the pressure gradient in front of the duct entrance. Since the ducts were designed to operate at an inlet-velocity ratio for high-speed flight of 0.65, the velocity of the air entering the ducts must be lower than the free-stream velocity. In order to decrease the velocity of the air as it flows along the ramp it is necessary for the air to flow from a region of lower static pressure at the ramp entrance to a region of higher static pressure at the duct entrance. The presence of the wing with its accompanying negative pressure field causes the region of low static pressure at the ramp entrance to become still lower so that the air must flow against a steeper pressure gradient along the ramp. This condition is conducive to a thickening of the boundary layer. To make this pressure gradient more gradual, a ramp that began ahead of the leading

edge of the wing was tested (ramp revision A). This is compared with the original ramp in figure 10. Ordinates for these ramps are given in table IV. The basic pressure distribution over the fuselage is shown in figure 11, and the ramp pressure gradients are shown in figure 12.

Originally, part of the boundary-layer air was removed at the duct entrance and exhausted through a slot at the bottom of the fuselage. Tests showed that a lower pressure was required at the boundary-layer duct exit to provide satisfactory boundary-layer removal. A 60° flap on the exit provided an entrance velocity ratio for the boundary-layer duct of approximately 0.7, regardless of the duct-entrance velocity ratio. This gave satisfactory boundary-layer removal, but, of course, too large an increase in drag. A complete series of tests was made with this system, however, as the data, corrected for the flap drag, could be used for any system that removed the same amount of boundary layer. The boundary layer could be pumped off, for example, by a jet-pump arrangement using the jet-motor exhaust. A stream-lined bump was then tested to provide a low pressure at the exit and a low drag simultaneously. This bump provided a boundary-layer-duct inlet-velocity ratio of about 0.5 for most conditions. Drawings of the original boundary-layer duct, the 60° exit flap, and the exit bump are presented in figure 13. A photograph of the bump is shown in figure 14. Tests were also made of a system that used no boundary-layer removal. This was done by fairing over the boundary-layer-duct entrances and exit. The ramp for this condition was called ramp revision B. The contour of the ramp is shown in figure 10; the pressure gradient for this contour is shown in figure 12. Ordinates are given in table IV.

Total-head profiles at the duct entrance are presented in figures 15 and 18. These show the effect of the ramp revisions, boundary-layer removal, angle of attack, and thrust coefficient. Some question may arise as to why the total-head profile for an inlet-velocity ratio of 0.34 is fuller than the profile for 0.54 in figure 15(a). One possible explanation is that a condition of unstable flow through the ducts exists so that one duct is operating at an inlet-velocity ratio less than 0.34, while the other is operating at an inlet velocity greater than 0.34. This unstable flow condition exists below an inlet-velocity ratio of 0.5 and is explained later on in the report.

Figure 15(b) shows the improvement obtained in the entrance profiles with revised ramp A and boundary-layer removal, while figure 15(c) shows the profiles obtained without boundary-layer removal. Figures 16(a) and 16(b) show the effect of boundary-layer removal for both right and left ducts, and figure 17 shows how the entrance profiles vary with angle of attack for an inlet-velocity ratio of 0.75. Entrance profiles with the propeller operating are presented in figures 18(a) and 18(b). The difference in the profiles for the right and left duct may be due to the effect of the propeller on the slipstream.

Pressure Recovery

The weight rate of air flow and the inlet-velocity ratio at 500 miles per hour of the General Electric I-40 unit are presented in figure 19 for sea level and 20,000 feet, as a function of pressure recovery at the face of the compressor. The pressure recovery of the original duct system was unsatisfactory due to the thick boundary layer present at the duct entrance, and the arrangement of the vanes in the diffuser. (See fig. 20.) In the revised diffuser the length of the vanes and the radius of curvature of the lower corner inside the diffuser were increased. The flow inside the diffuser was investigated by means of a probe with a small tuft on the end. This made it possible to view the flow characteristics through the transparent walls used in the construction of the diffuser for the bench tests. The bench-test apparatus is shown in figure 21. In the final diffuser the radius of curvature of both the upper and lower corners was increased and the vanes to turn the air were eliminated. It was necessary, however, to install three vanes near the lower surface of the diffuser to keep the air flow from separating from the surface.

The pressure recovery for the final revised diffuser in combination with various boundary-layer-removal systems is presented in figure 22. Data are presented also in figure 22 for a configuration in which the ramp diverged as it approached the duct entrance. This divergent ramp was designed to approximately fit the streamlines for the high-speed inlet-velocity ratio as indicated by the pressure gradient ahead of the opening. A photograph and a drawing of this ramp are presented in figures 23 and 24, respectively. Apparently the divergent

ramp reduced the thickness of the boundary layer present at the entrance, although the data taken were not complete enough to check this. The ramp was tested only for the faired-over condition of the boundary-layer ducts. Figure 25 shows the effect of propeller operation and inlet-velocity ratio on static pressure recovery in the plenum chamber with and without boundary-layer removal.

Internal and External Drag

In order to calculate the speed of an airplane, it is only necessary to know two things: (1) total thrust, and (2) total drag. Total thrust for a jet-propelled airplane depends only on the pressure ahead of the compressor for given operating conditions (rpm, altitude). Total drag is the sum of the external drag and the momentum or ram drag. Momentum or ram drag is defined as the force that is produced due to bringing all the air which enters the ducts to a stop in the drag direction. Total drag is measured on the wind-tunnel balances when the air entering the model is removed from the tunnel at 90° to the drag direction.

In general, the external drag can be found by subtracting the free-stream momentum of the entering air from the total drag. In coefficient form the internal drag may be written

$$C_{D_{int.}} = 2\left(\frac{A}{S}\right)\left(\frac{V_A}{V_o}\right)$$

where

A/S $\frac{\text{duct entrance area}}{\text{airplane wing area}}$

V_A/V_o duct inlet-velocity ratio

In the present case, however, this is not consistent with the definition of external drag. External drag has been defined as the drag due to the exterior portion of the airplane, so that the loss in momentum, due to friction, suffered by the air passing over the fuselage before entering the duct system

cannot be charged to internal drag. This loss of free-stream momentum was evaluated by measuring the total-head profiles of the entering air. The conditions at the duct entrance were evaluated from free-stream static pressure, and the free-stream momentum corresponding to the entrance momentum was found. The internal drag was then

$$C_{D_{int.}} = 2\left(\frac{A}{S}\right)\left(\frac{V_A}{V_O}\right)\sqrt{\frac{H_A - p_o}{q_o}}$$

where $\sqrt{\frac{H_A - p_o}{q_o}}$ is the average value of the quantity across the duct entrance. This correction is developed more fully in the appendix.

Total drag curves plotted against angle of attack are given in figures 26(a) to 26(g), for inlet-velocity ratios of $V_A/V_o = 0$ to $V_A/V_o = 1.4$. These data are cross-plotted for $\alpha = 0$ in figure 27. If the internal drag coefficient is subtracted from the total drag coefficient, the resulting value is the external drag coefficient. The variation of external drag coefficient with inlet-velocity ratio is presented in figure 28 for $\alpha = 0^\circ$.

If a line is drawn on figure 27 with the slope $2(A/S)$ and passing through $C_{D_{total}} = 0.0165$ at $V_A/V_o = 0$, the curve for "dragless" ducts that take in no boundary layer will result. As the actual I-40 air-intake ducts do have drag, and as boundary-layer air is used, the various configurations have a higher drag and a smaller slope than this curve. Above an inlet velocity of 0.55 though, two of the curves for the configuration, in which all the boundary layer is taken into the plenum chamber, drop below the curve for dragless ducts. One explanation of this may be that the ducts which take in most of the boundary layer reduce the drag of the fuselage by an amount which is sufficient to more than offset the drag of the ducts themselves. Thus, less drag is obtained with the ducts that take in the boundary layer than in the hypothetical case of the dragless ducts which take in no boundary layer.

Calculations to compare the relative merits of the various duct systems for high-speed flight are given in table V.

It was determined from data on the I-40 unit that a decrease in pressure recovery of $0.10q_0$ resulted in a loss in thrust equivalent to an increase in drag coefficient of $\Delta C_D \cong 0.0008$ for the sea-level high-speed condition. A comparison of the various systems was made on this basis, using the hypothetical case of the fuselage with dragless ducts that take in no boundary layer and that have 100-percent pressure recovery as the base with which the other systems are compared.

It should be borne in mind that the drag data presented herein are low Mach number data, and as the ducts have a low critical Mach number, the duct drag may be much higher in the high-speed condition.

Unstable Flow

Considerable difficulty was caused throughout these tests by an unstable flow condition through the ducts at low inlet-velocity ratios. At a certain inlet-velocity ratio, depending upon the configuration, the flow through the two ducts would suddenly become unsymmetrical. The flow stopped in one of the ducts, or actually reversed, while all the flow went through the opposite duct. This produced a sudden drop in pressure recovery, and a large increase in drag. Apparently separation along the ramp was responsible for this. The process can be explained as follows:

As the inlet-velocity ratio is decreased, more air must flow around and over the top of the ducts. A steeper and more unfavorable pressure gradient occurs along the ramp as there is an increasing difference between the pressure at the ramp entrance and the pressure at the duct inlet. The pressure at the ramp entrance remains approximately the same while the pressure in front of the duct inlet becomes higher as the inlet-velocity ratio is decreased. The decreasing inlet-velocity ratio will cause the boundary layer to become thicker so that a point may be reached when separation will occur along the ramp. Since the flow along both ramps will never be quite symmetrical, separation will not occur along both ramps simultaneously. The separation of the flow along one ramp may reduce the total head at the duct entrance below that in the plenum chamber so that the air may actually reverse through the duct.

Thus, at an over-all inlet-velocity ratio of 0.4, one duct may be operating at $V_A/V_o \cong 1.0$ and the other at $V_A/V_o \cong -0.2$. Examples of the effects of unstable flow can be seen in figures 15(a), 22, and 28. Figure 15(a) indicates unsymmetrical flow because the total-head profile at the entrance of the right duct for an inlet-velocity ratio of 0.34 is fuller than the profile for an inlet-velocity ratio of 0.54. This would indicate that this duct was operating at an inlet-velocity ratio considerably greater than the average value of 0.34, while there is probably little if any air flowing through the other duct. The sudden drop-off in the recovery pressure coefficient at an inlet-velocity ratio of 0.5 in figure 22 and the increase in drag below an inlet-velocity ratio of 0.5 in figure 28 are also indicative of unstable flow conditions. The configurations with boundary-layer ducts faired over were considerably more stable than the configurations using boundary-layer removal.

A condition of very high drag and high external pressures over one duct may actually become dangerous, as it is quite possible to obtain low inlet-velocity ratios in a high-speed dive. Several solutions to this problem are possible. The ducts may be blocked internally or externally when the unit is not in use. The plenum chamber may be divided so that air cannot flow from one duct to the other. If smaller ducts with higher inlet-velocity ratios are used, low enough flows may not occur in flight to cause this instability.

CONCLUSIONS

The results of the tests of the I-40 air-intake duct system indicate the following:

1. It is not possible with the duct system tested to secure a sufficiently high critical Mach number with the ducts in their present position and operating at an inlet-velocity ratio of less than 1.0.

2. To secure high pressure recovery without increasing the external drag simultaneously it is necessary to find some other means of boundary-layer removal at the duct entrance; for instance, using the I-40 jet-motor exhaust as a jet pump to remove the boundary layer.

3. On the airplane model tested, the low drag and simplicity of a duct system that uses the boundary layer are more important than the high pressure recovery of a system that removes all, or part of, the boundary layer.

4. A duct system using a streamlined bump on the boundary-layer exit duct provided the smallest decrease in thrust as compared with a system that had dragless ducts having 100-percent pressure recovery and taking in no boundary layer.

Ames Aeronautical Laboratory,
National Advisory Committee for Aeronautics,
Moffett Field, Calif.

APPENDIX

DERIVATION OF INTERNAL DRAG COEFFICIENT

In bringing air to a stop, or in changing its direction by 90°, a drag is incurred. This drag may be written

$$D = \rho_o Q V_o$$

where

ρ_o atmospheric density, slugs per cubic foot

Q quantity of air considered, cubic feet per second

V_o free-stream velocity, feet per second

When applied to an airplane this may be written in coefficient form:

$$C_{D_{int.}} = 2 \left(\frac{A}{S}\right) \left(\frac{V_A}{V_o}\right)$$

where

A/S $\frac{\text{duct entrance area}}{\text{airplane wing area}}$

V_A/V_o $\frac{\text{duct entrance velocity}}{\text{free-stream velocity}}$

In general, this may be used as an indication of the internal drag when testing wind-tunnel models, so that the external drag of various configurations may be compared. For a duct system in which there is boundary layer present at the duct entrance the internal drag as defined in the preceding equation will include part of the external drag of the airplane, making the correction no longer accurate.

In the present case, part of the free-stream momentum has been lost before the air enters the ducts. This loss is part of the external drag, so that it is necessary to evaluate how much of the original free-stream momentum is lost as the

air passes over the surface of the fuselage to reach the duct. This loss is due to the formation of a boundary layer which causes the average total pressure at the duct entrance to be less than the free-stream total pressure. If the conditions at duct entrance are extrapolated to free-stream conditions by Bernoulli's equation, the momentum for an element of area at the duct entrance may be written:

$$\text{momentum} = m\,v\,dA$$

where

m mass flow per element of area, slugs per second per unit area

v velocity of flow of the air based on the total head at the element of area and free-stream static pressure, feet per second

dA the area of the element of area

If h is the duct height, b the duct width, dy the height of any element of area, and v is assumed constant across the duct width

$$D_{int.} = b\int_0^h mv\,dy$$

$$= b\int_0^h \rho_A V_A\,v\,dy$$

$$= b\int_0^h \rho_A V_A \sqrt{\frac{2(H_A - p_o)}{\rho_o}}\,dy$$

where

p_o free-stream static pressure, pounds per square foot

ρ_o free-stream density, slugs per cubic foot

ρ_A density at duct entrance, slugs per cubic foot

V_A velocity of flow through element of area, feet per second

$\sqrt{\frac{2(H_A - p_o)}{\rho_o}}$ equivalent free-stream velocity where H_A is total head at duct entrance, pounds per square foot

If $b\int_o^h \rho_A V_A \sqrt{\frac{2(H_A - p_o)}{\rho_o}}\, dy$ is divided by the free-stream dynamic pressure and the airplane wing area, and reduced to coefficient form, the following equation will result:

$$C_{D_{int.}} = \frac{b}{q_o S}\int_o^h \rho_A V_A \sqrt{\frac{2(H_A - p_o)}{\rho_o}}\, dy$$

$$= \left(\frac{2A}{S}\right)\left(\frac{V_A}{V_o}\right)\left(\frac{\rho_A}{\rho_o}\right)\sqrt{\frac{\overline{(H_A - p_o)}}{q_o}}$$

where the bar indicates the mean value of the term. The mean value of the term $\sqrt{\frac{\overline{(H_A - p_o)}}{q_o}}$ was found by plotting values of the term measured at the duct center line, and integrating with a planimeter. The average value of the term V_A/V_o over the duct area was found by dividing the Venturi-measured quantity of flow by the duct-entrance area. Values of these terms and corresponding internal drag coefficients are given in table VI for the various configurations. The term ρ_A/ρ_o may be considered to be equal to one for low velocities.

REFERENCE

1. Allen, H. Julian, and Vinconti, Walter G.: Wall Interference in a Two-Dimensional-Flow Wind Tunnel with Consideration of the Effect of Compressibility. NACA ARR 4K03, 1944.

TABLE I.- DIMENSIONS OF THE 1/4-SCALE STUB-WING MODEL OF A PURSUIT-TYPE AIRPLANE.

Stub-wing area	22.23	square feet
Stub-wing chord	3.27	feet
1/4-scale-wing area	26.55	square feet
Cowl-intake area	0.0781	square feet
Original duct-intake area	0.1475	square feet
Revised duct-intake area	0.1420	square feet

TABLE II.- AIRFOIL ORDINATES OF THE WING USED ON THE AIRPLANE

(The airfoil is a modified $65_{(112)}$-213 (a = 1). The upper surface aft of 75 percent chord is a straight line, tangent at 75 percent chord and trailing-edge radius. The lower surface aft of 60 percent is a straight line, tangent at 60 percent and trailing-edge radius.)

(Abcissas and ordinates in percent of wing chord)

Station	Upper surface	Lower surface
0.5	1.135	0.888
.75	1.341	1.070
1.25	1.665	1.347
2.5	2.272	1.820
5	3.180	2.485
7.5	3.898	2.985
10	4.496	3.407
15	5.458	4.082
20	6.192	4.578
25	6.755	4.955
30	7.163	5.214
32	7.282	5.293
35	7.430	5.372
40	7.563	5.425
45	7.536	5.348
50	7.338	5.135
55	6.956	4.770
60	6.425	4.284
65	5.780	3.755
67	5.488	3.548
70	5.038	3.232
73	4.555	2.918
75	4.223	2.705
80	3.388	2.176
85	2.558	1.647
90	1.732	1.119
95	.901	.591
100	-----	-----

Leading-edge radius: 1.1735. Leading-edge radius above chord plane: 0.10. Trailing-edge radius: 0.064.

TABLE III.- ORDINATES OF THE TOP CENTER LINE OF THE FINAL I-40 AIR-INTAKE DUCT (FULL SCALE)

Station (in.)	Ordinate from top center line to duct reference line (in.)
279.22	32.63 (0.375R on lip)
282.38	34.66
286.75	35.78
291.13	36.37
300.00	36.83
309.00	36.73
318.00	36.10
323.75	35.44
333.25	33.92
342.75	31.90
351.75	29.55
356.25	28.30
362.00	26.76
366.00	25.76
376.00	23.45
386.00	21.58
396.00	20.33
406.00	19.52
416.00	18.70

TABLE IV.- RAMP ORDINATES OF THE AIR INTAKE DUCTS FOR THE I-40 JET PROPULSION ENGINE

(Ordinates are given in inches, full scale, from the duct reference line)

Full-scale station (in.)	Original ramp	[1] Ramp revision A	[2] Ramp revision B
191	-------	27.74	27.74
198.5	-------	-------	27.58
201.75	-------	27.5	------
206	-------	-------	27.27
210.75	-------	26.995	------
213.5	-------	-------	26.87
220.875	27.715	26.080	------
221	-------	-------	26.38
228.5	-------	-------	25.84
229.625	27.447	25.050	------
236	-------	-------	25.25
238.375	26.830	23.900	------
243.5	-------	-------	24.63
247.125	25.830	22.745	------
251	-------	-------	24.01
255.875	24.570	21.605	------
258.5	-------	-------	23.40
264.5	23.065	20.605	------
266	-------	-------	22.85
273.5	-------	-------	22.39
274	21.125	19.880	------
279	-------	19.617	------
281	19.536	-------	22.13

[1] Consists of the aft 60 percent of an NACA 65(216)-0(10.4) airfoil.

[2] Consists of the aft 60 percent of an NACA 64(215)-0(8.78) airfoil.

TABLE V.- COMPARISONS OF DUCT SYSTEMS FOR THE HIGH-SPEED FLIGHT CONDITION
($V_A/V_o = 0.65$, $\alpha = 0^o$)

Configuration	Pressure recovery, $\frac{P_B - p_o}{q_o}$	$\frac{\Delta(p_B - p_o)}{q_o}$	$\frac{-(0.0080)\times\Delta(p_B - p_o)}{q_o}$	$C_{D_{total}}$	$\Delta C_{D_{total}}$	$\Delta C_{D_{total}} + 0.0080 \times \frac{\Delta(p_B - p_o)}{q_o}$	Change in thrust at 500 mph (lb)
Fuselage with "dragless" ducts considered as base	1.00	0	0	0.0235	0	0	0
60° boundary-layer exit flap	.71	-.29	.0023	.0284	.0049	.0072	-1950
60° boundary-layer exit flap with flap drag subtracted	.71	-.29	.0023	.0244	.0009	.0032	-870
Boundary-layer exit bump	.64	-.36	.0029	.0240	.0005	.0034	-920
Boundary-layer ducts faired over, straight-walled ramp	.36	-.64	.0051	.0233	-.0002	.0049	-1330
Boundary-layer ducts faired over, divergent walled ramp	.48	-.52	.0042	.0231	-.0004	.0038	-1030

TABLE VI.- INTERNAL-DRAG COEFFICIENTS ($\alpha = 0^\circ$)

Configuration	V_A/V_o	$\sqrt{\frac{(H_A-p_o)}{q_o}}$	$C_{D_{int.}}$
60° boundary-layer exit flap	0.36	0.92	0.0036
	.56	.96	.0058
	.76	.97	.0079
	.93	.98	.0098
Boundary-layer exit bump	.36	.93	.0036
	.56	.92	.0056
	.93	.97	.0096
Boundary-layer ducts faired over, straight-walled ramp	.36	.72	.0028
	.56	.82	.0049
	.75	.87	.0070
	.94	.89	.0089
Boundary-layer ducts faired over, divergent ramp	.18	.62	.0012
	.36	.69	.0024
	.56	.83	.0050
	.75	.89	.0071
	.93	.91	.0091

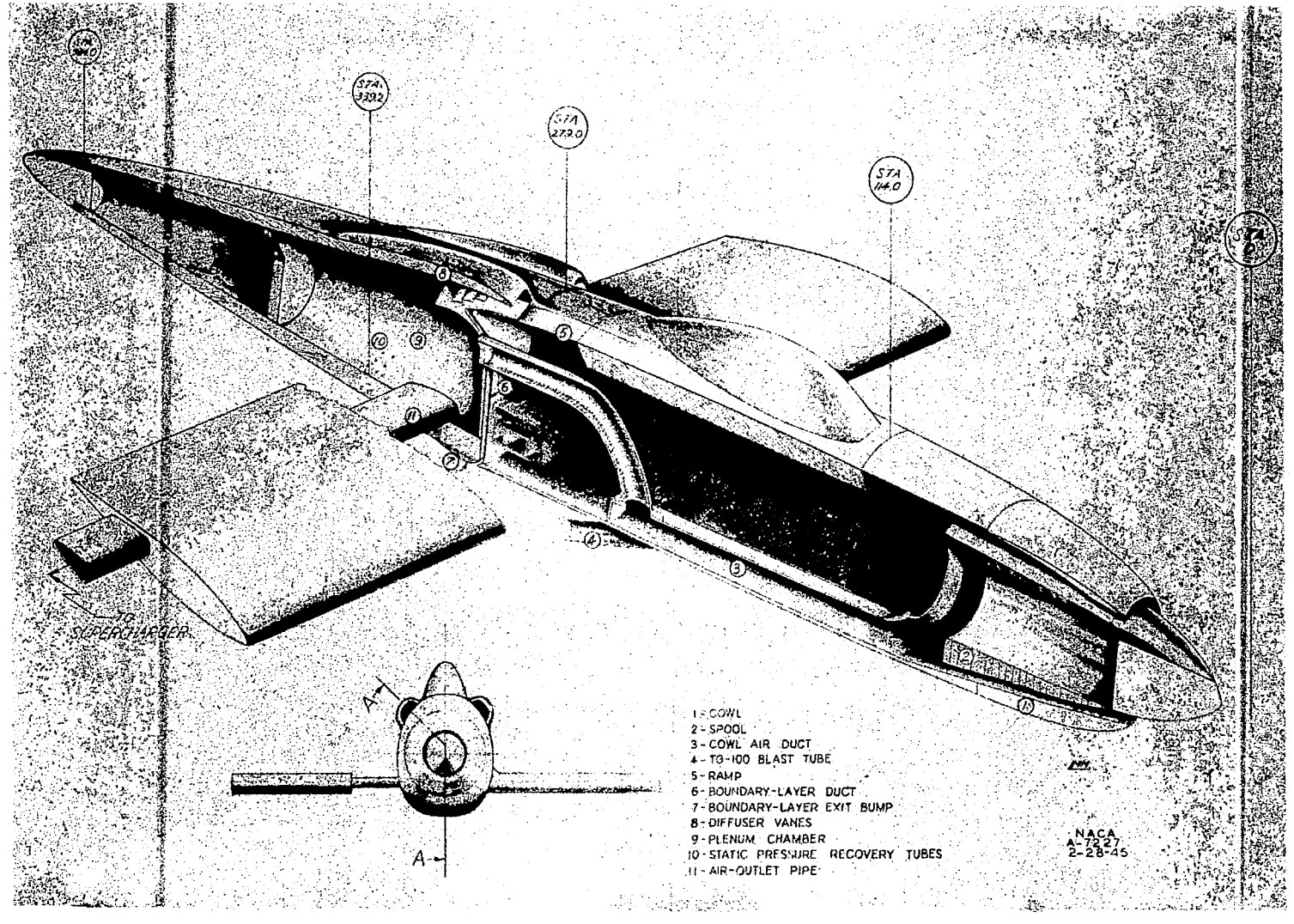

Figure 1.- Sectional view of 1/4-scale stub-wing model of the airplane

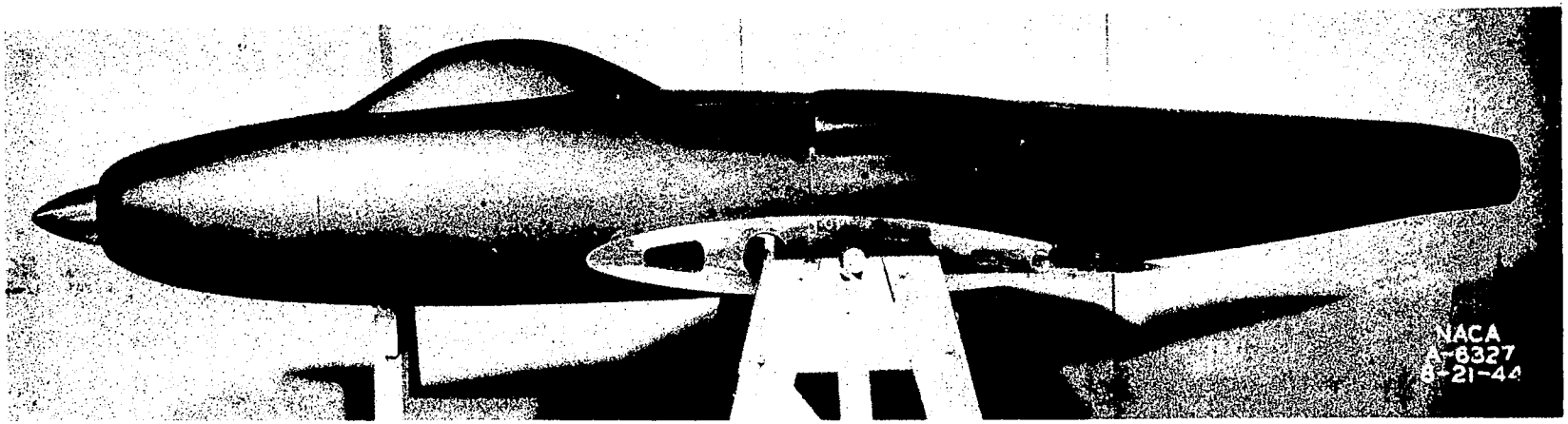

Figure 2.- Side view of 1/4-scale stub-wing model of the airplane showing original I-40 air-intake ducts.

Figure 3.- Original I-40 air-intake ducts showing boundary-layer removal ducts. The 1/4-scale stub-wing model of the airplane.

Figure 4.- The 1/4-scale stub-wing model of the airplane mounted in the Ames 7- by 10-foot wind tunnel.

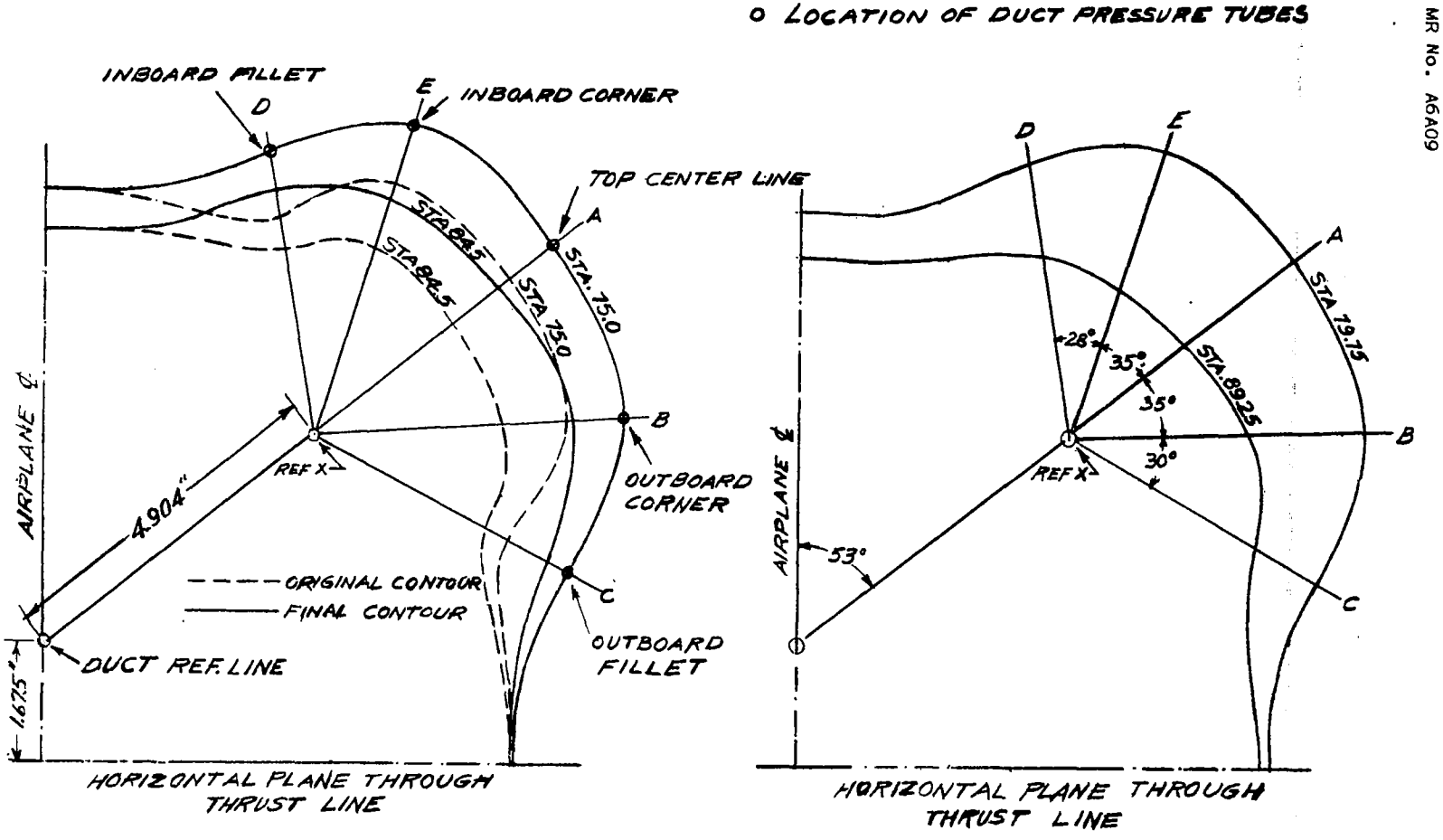

(a) CROSS-SECTION VIEWS

FIGURE 5. - ORIGINAL AND FINAL EXTERIOR CONTOURS OF THE DUCTS ON THE 1/4-SCALE STUB-WING MODEL.

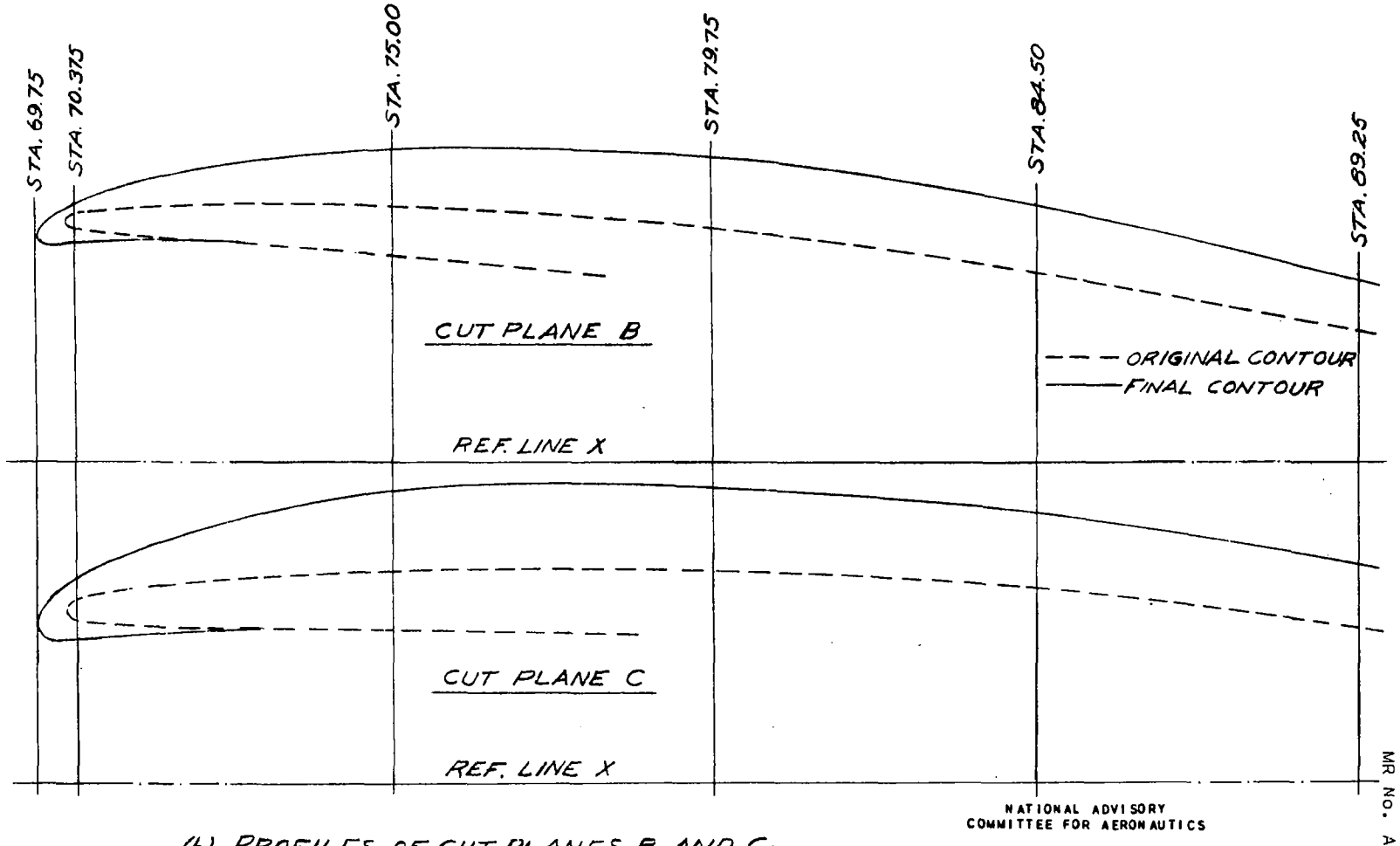

(b) PROFILES OF CUT PLANES B AND C.

FIGURE 5.- CONTINUED

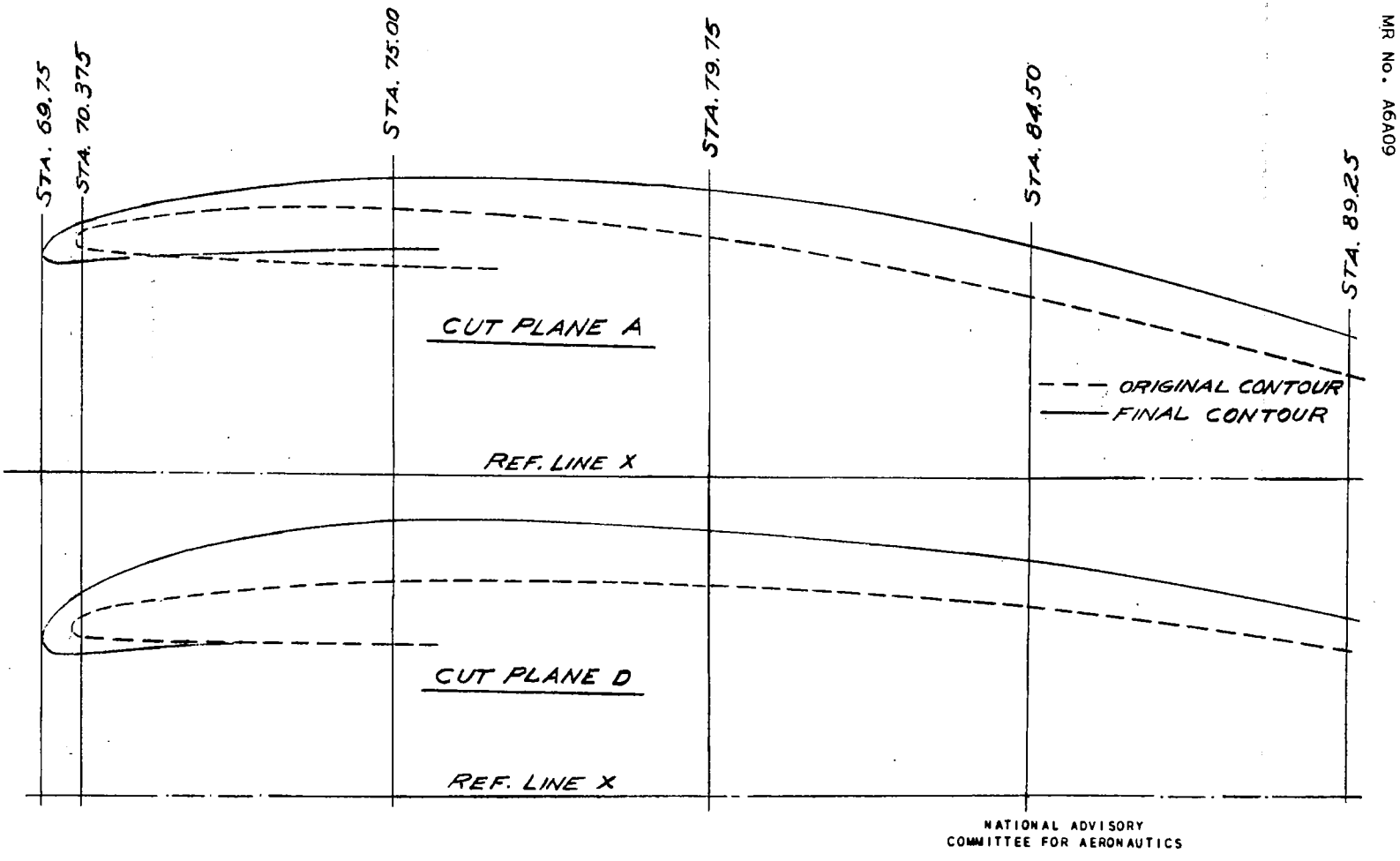

(c) PROFILES OF CUT PLANES A AND D

FIGURE 5.- CONCLUDED.

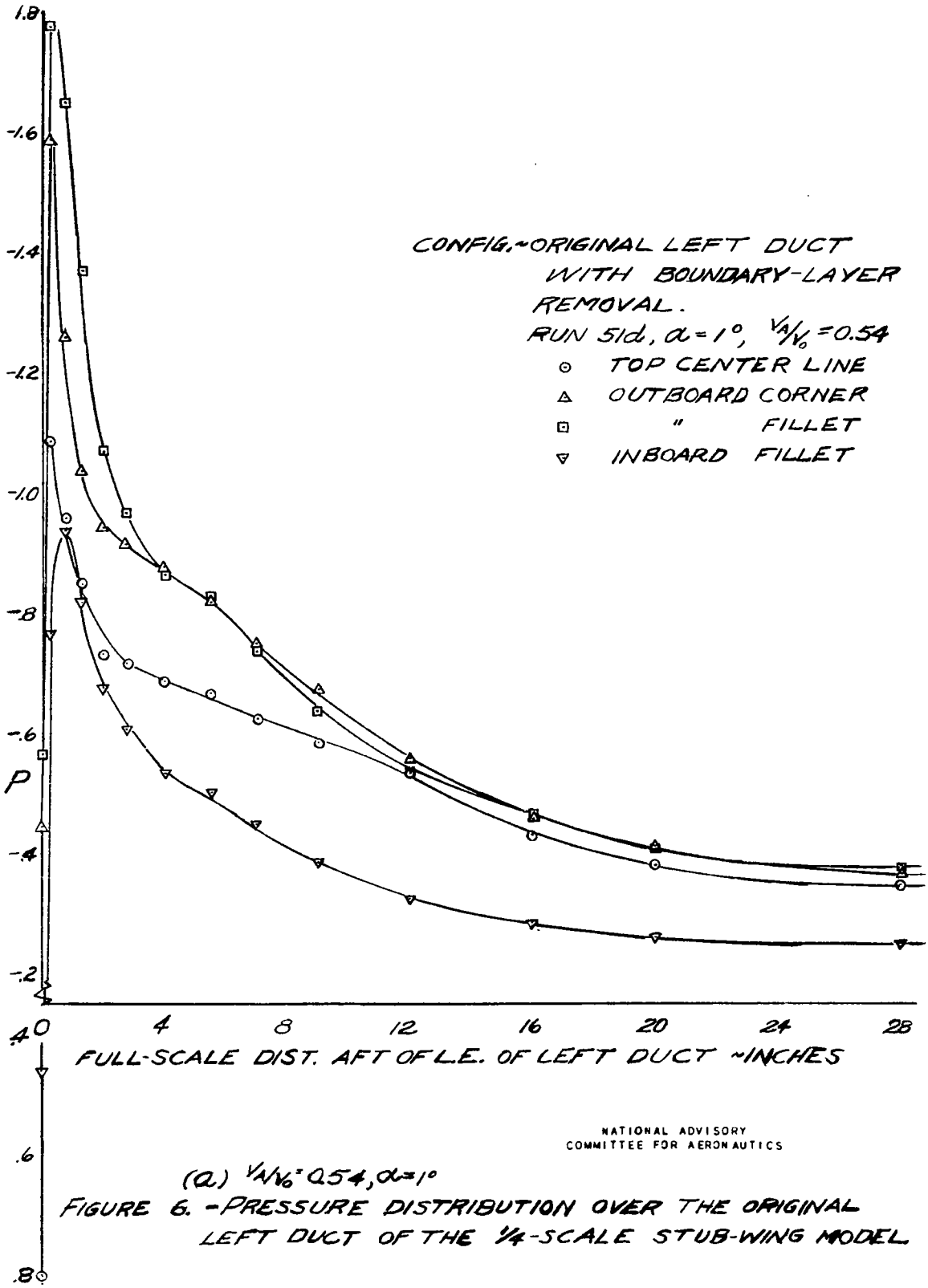

NATIONAL ADVISORY
COMMITTEE FOR AERONAUTICS

(a) $V_A/V_0 = .54$, $\alpha = 1°$

FIGURE 6. -PRESSURE DISTRIBUTION OVER THE ORIGINAL LEFT DUCT OF THE 1/4-SCALE STUB-WING MODEL

MR No. A6A09

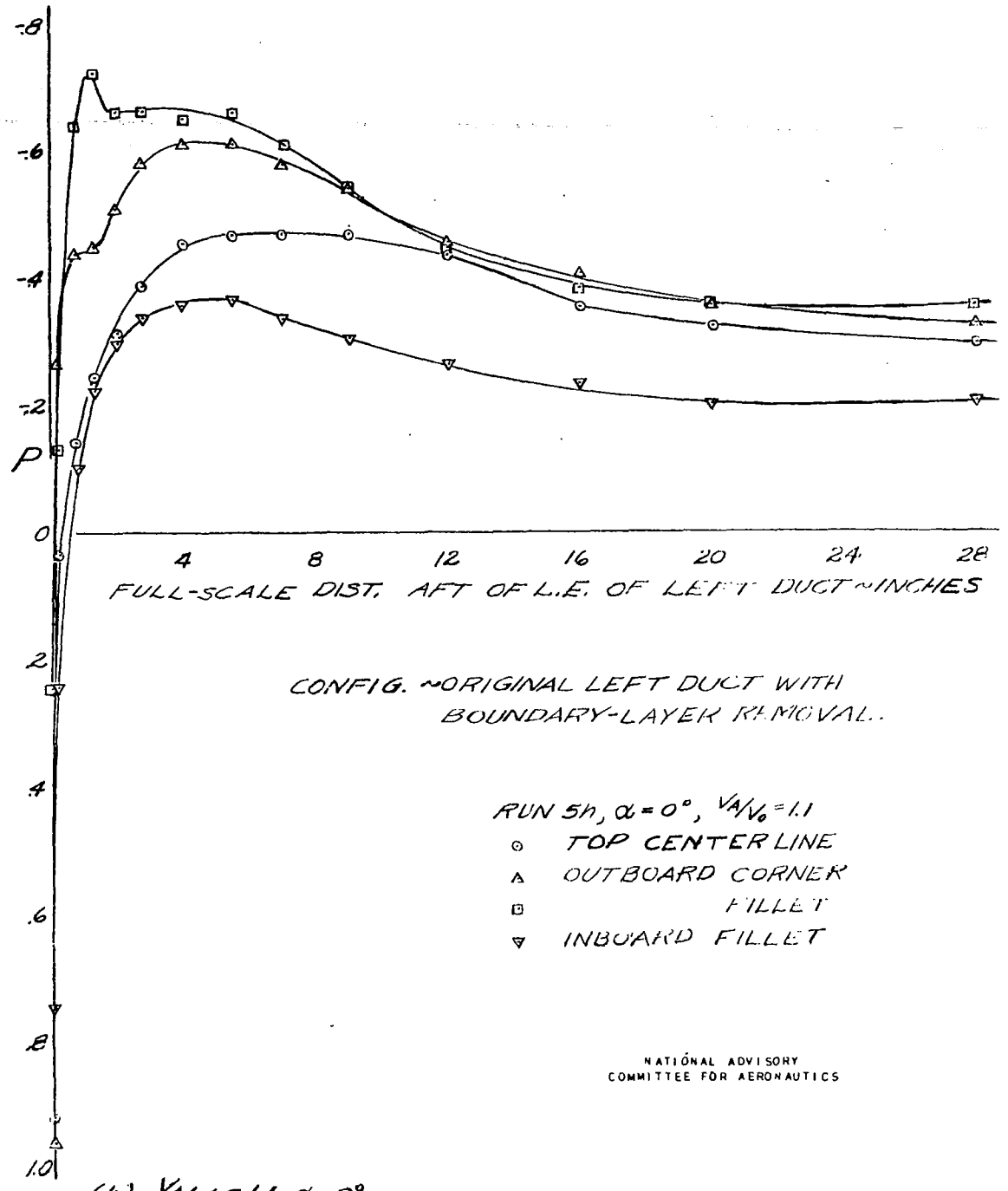

(b) $V_A/V_0 = 1.1$ $\alpha = 0°$

FIGURE 6. – CONCLUDED.

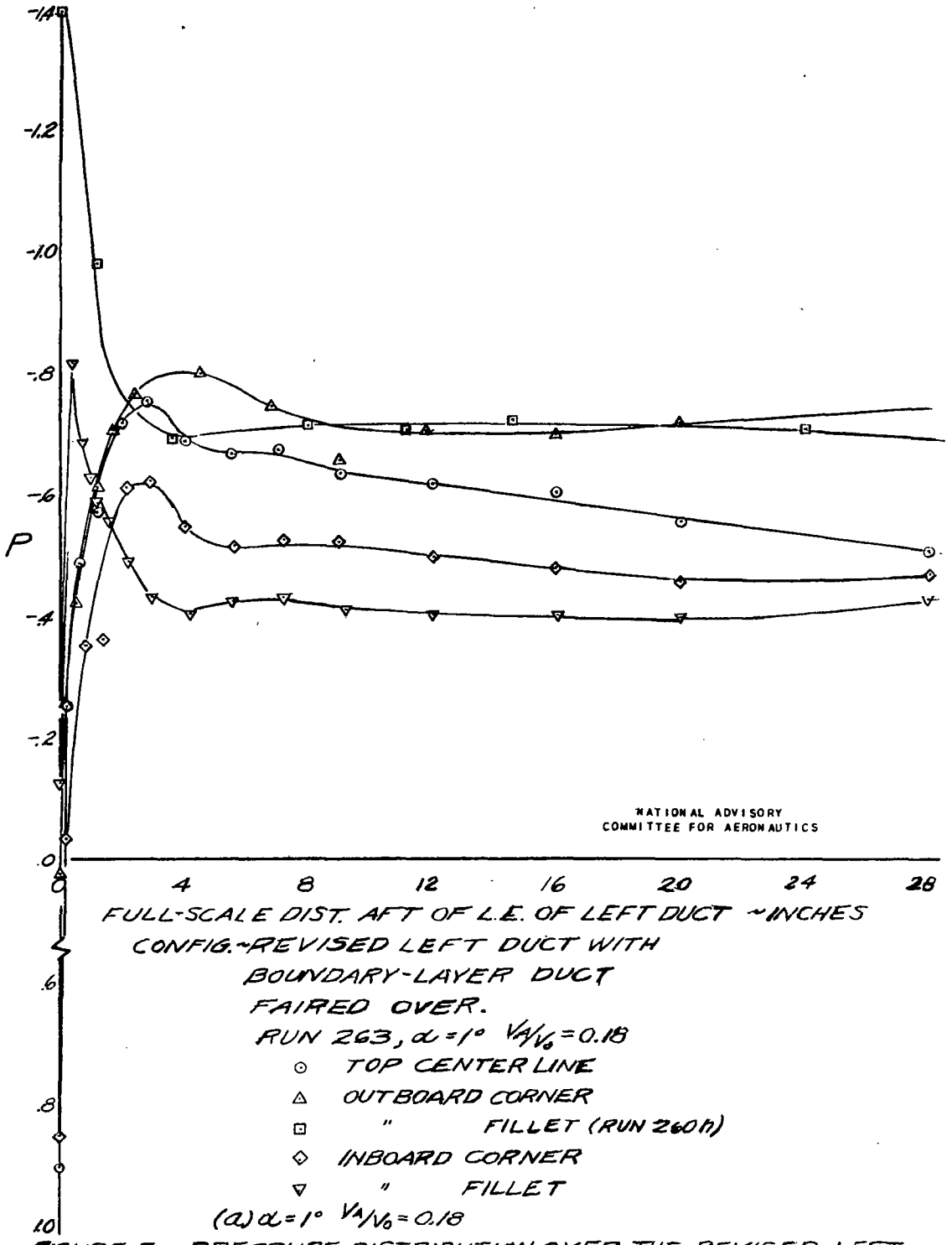

FIGURE 7.- PRESSURE DISTRIBUTION OVER THE REVISED LEFT DUCT OF THE 1/4-SCALE STUB-WING MODEL.

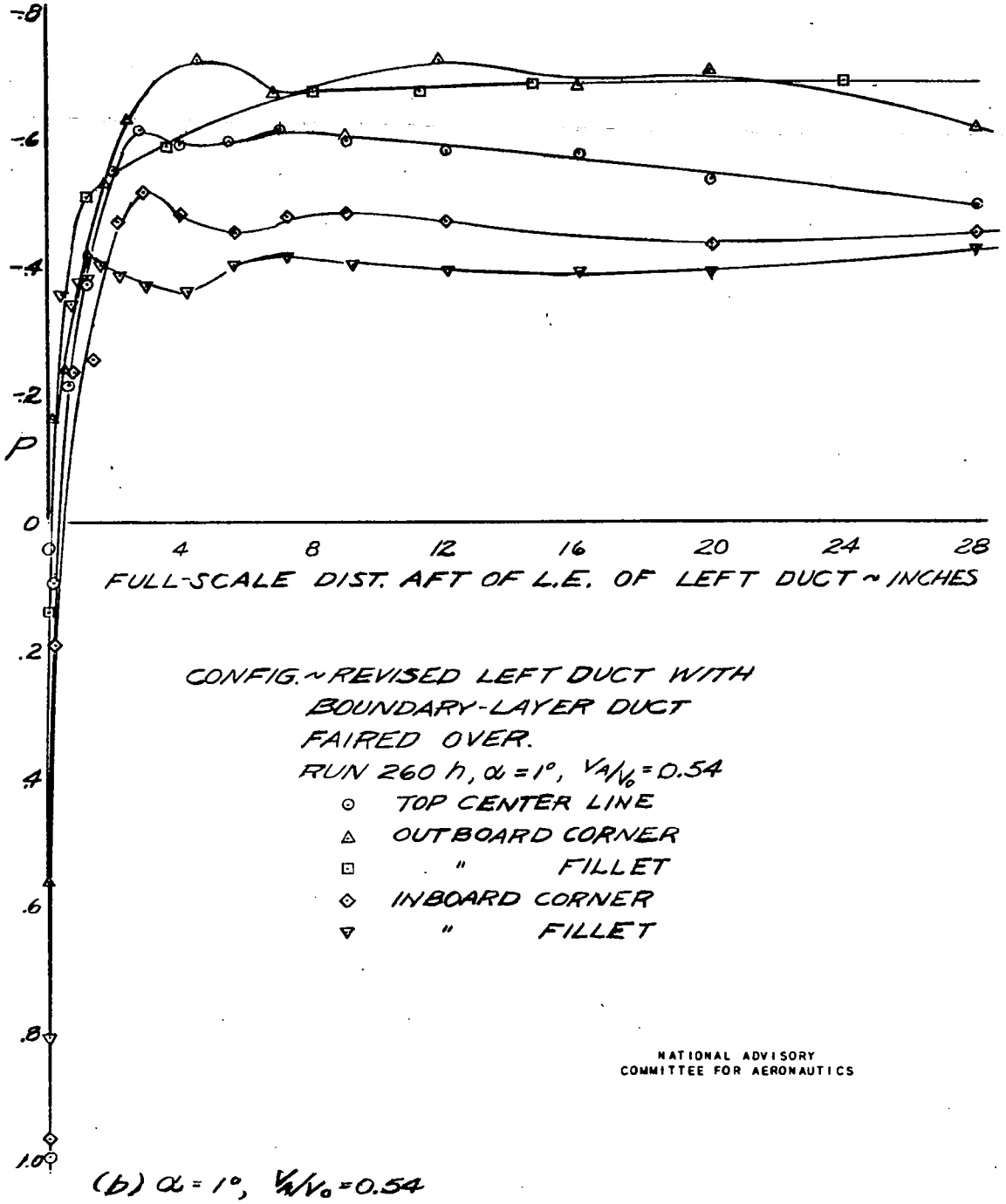

(b) $\alpha = 1°$, $V_A/V_0 = 0.54$

FIGURE 7. - CONTINUED.

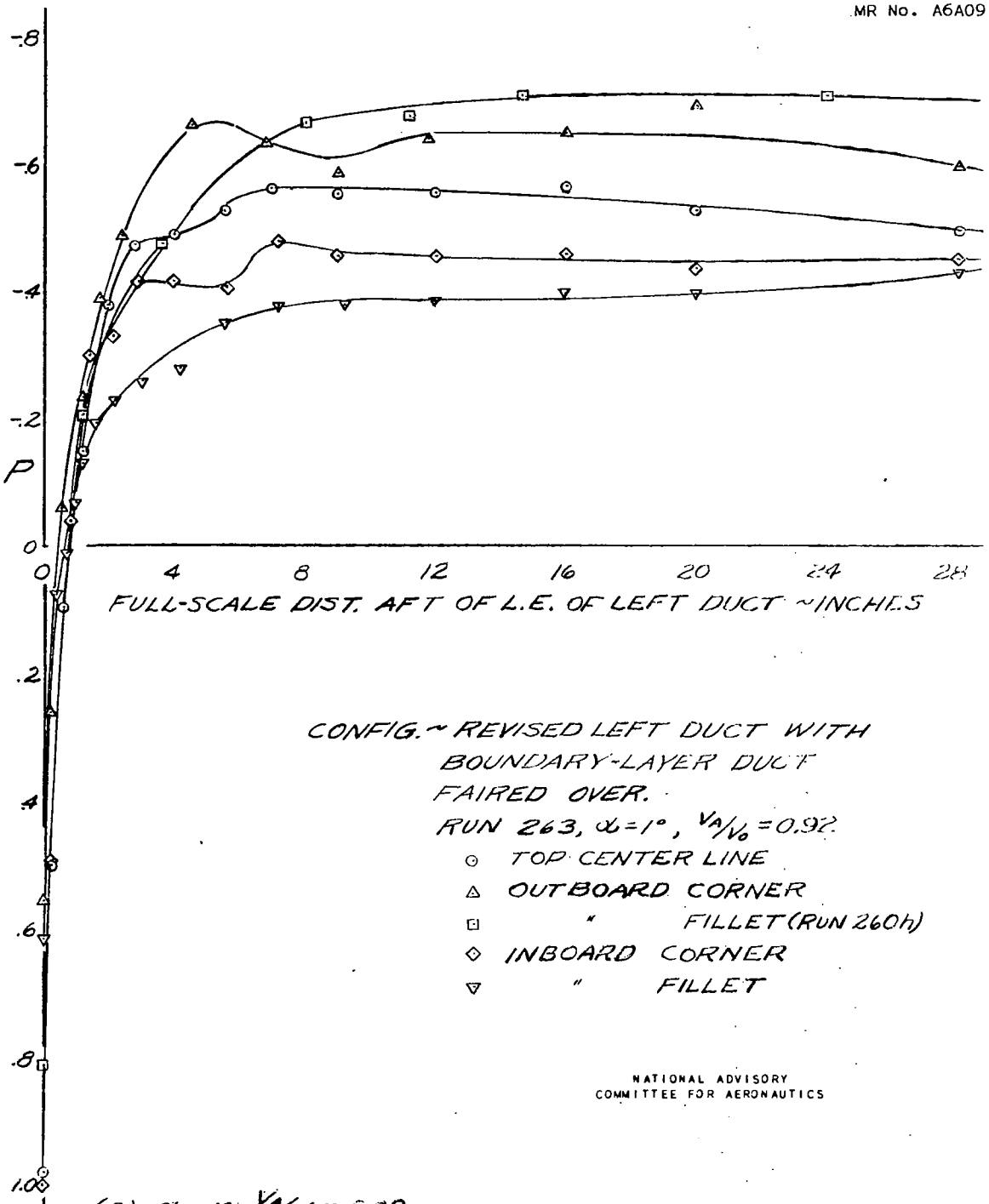

(C) $\alpha = 1°$, $V_A/V_0 = 0.92$

FIGURE 7. - CONTINUED

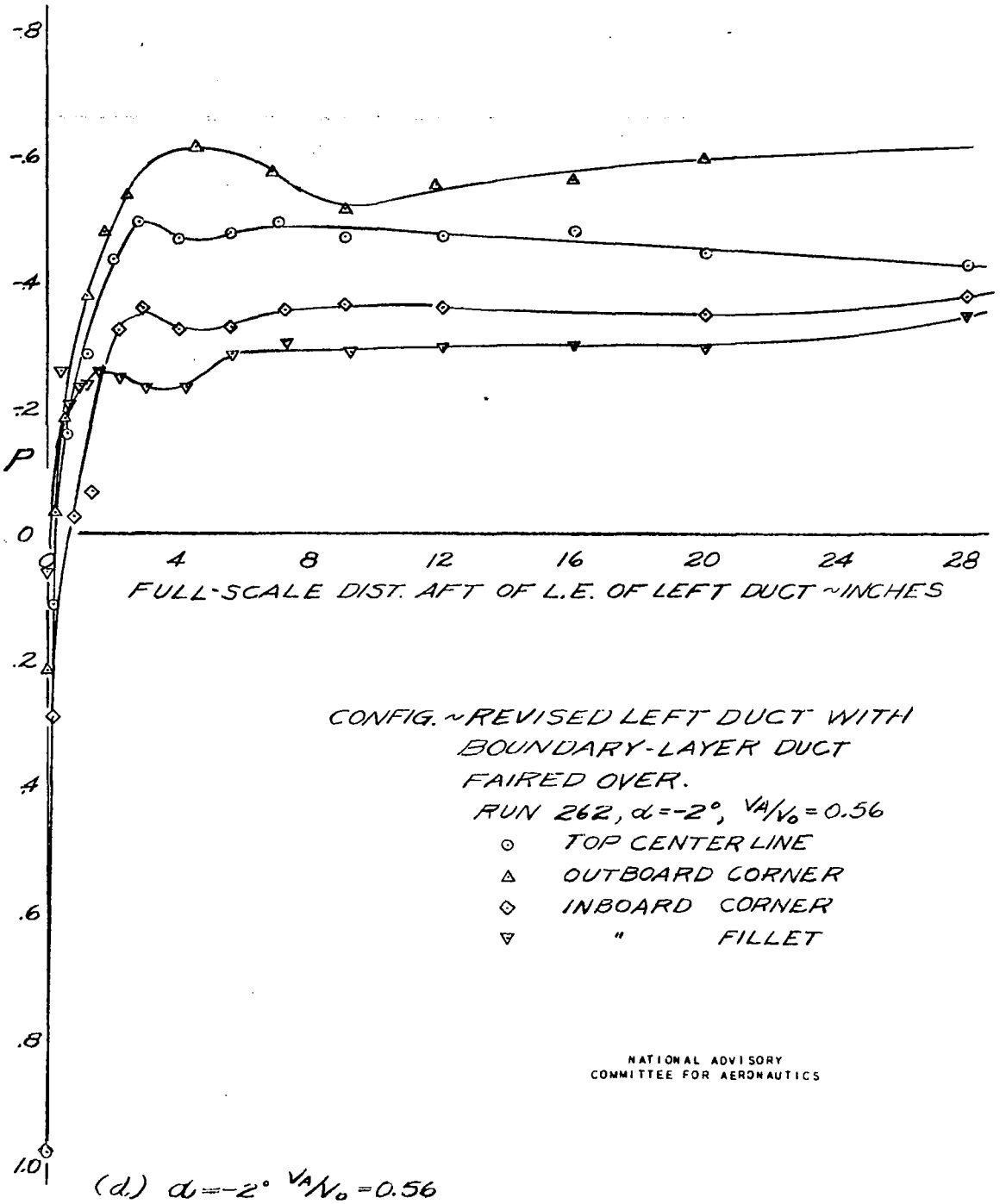

(d.) $\alpha = -2°$ $V_A/V_o = 0.56$

FIGURE 7. - CONTINUED.

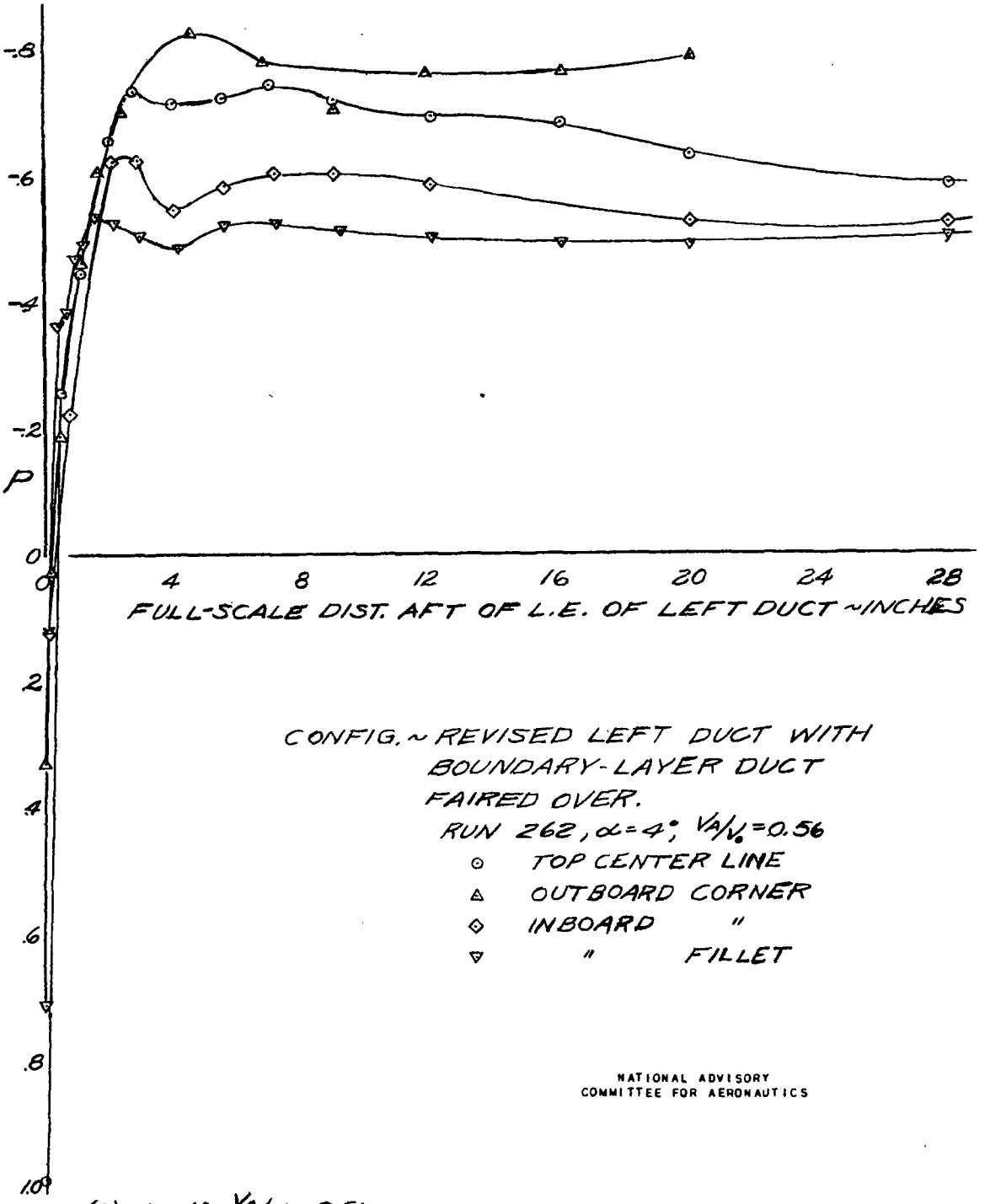

(e) $\alpha = 4°$ $V_A/V_0 = 0.56$

FIGURE 7. - CONCLUDED.

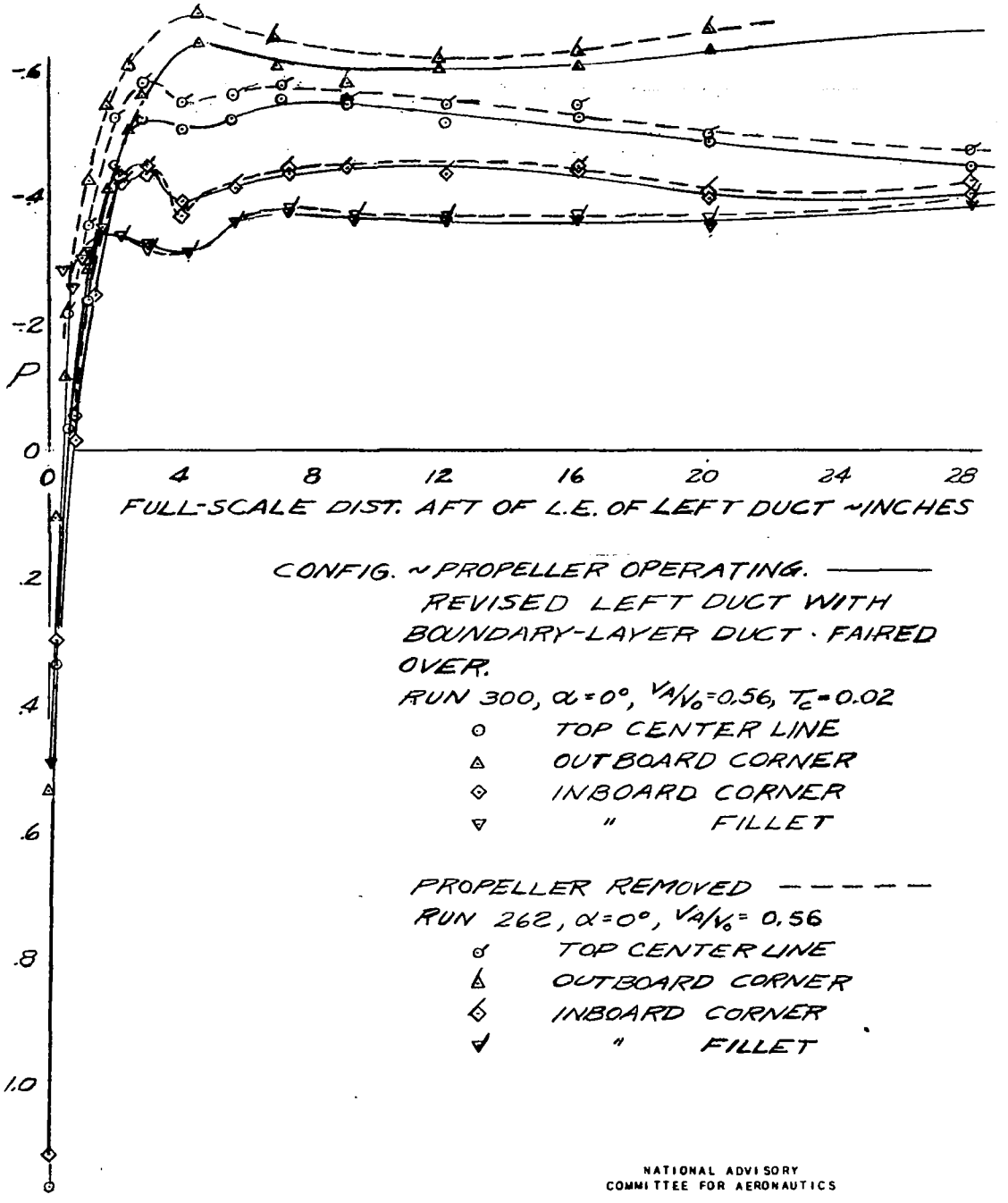

FIGURE 8.-PRESSURE DISTRIBUTION OVER THE REVISED LEFT DUCT; PROPELLER OPERATING, $\alpha = 0°$; $V_A/V_0 = 0.56$, $T_c = 0.02$; PROPELLER REMOVED, $\alpha = 0°$, $V_A/V_\infty = 0.56$

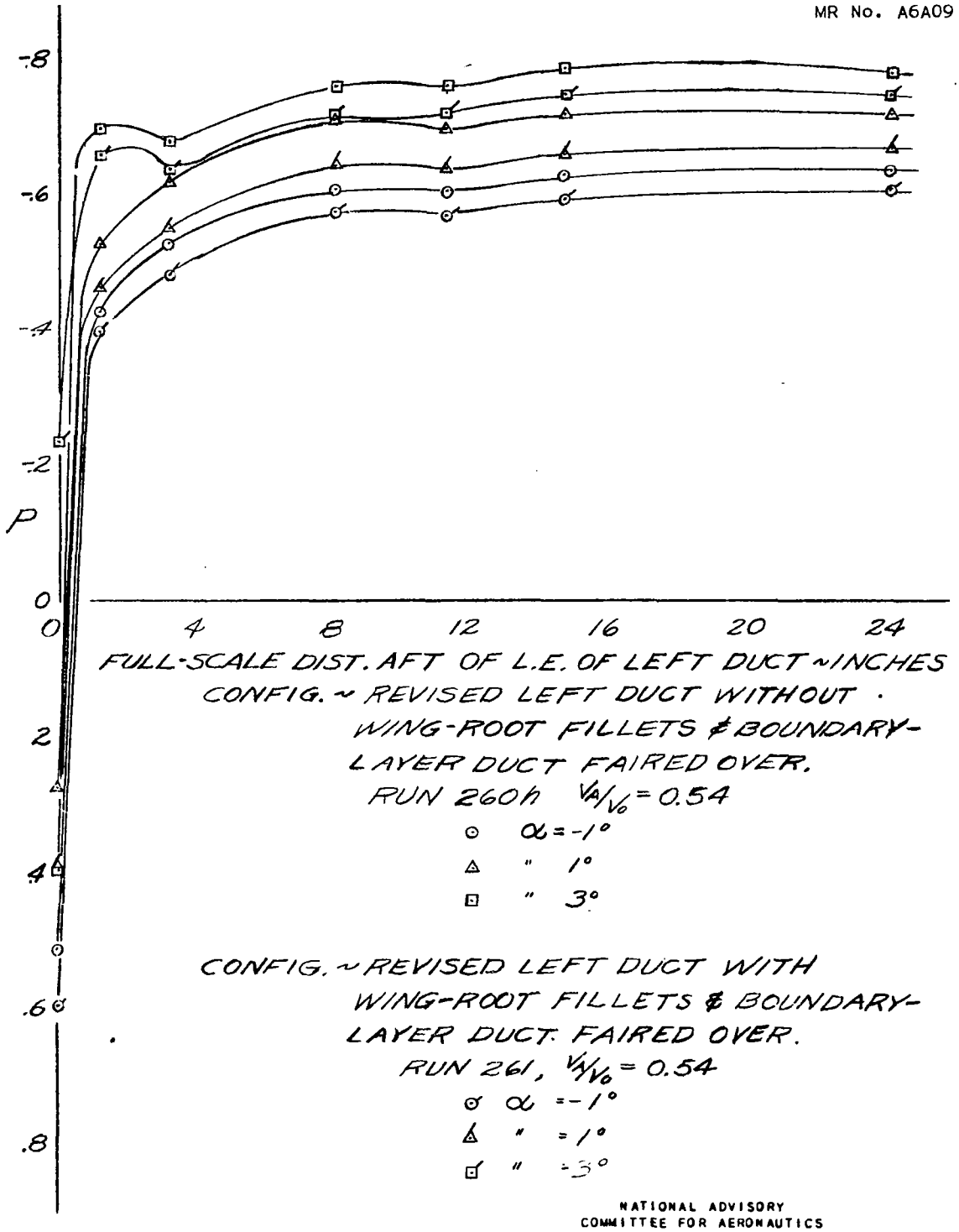

FIGURE. 9. - PRESSURE DISTRIBUTION OVER THE OUTBOARD FILLET OF THE REVISED LEFT DUCT WITH AND WITHOUT WING-ROOT FILLETS.

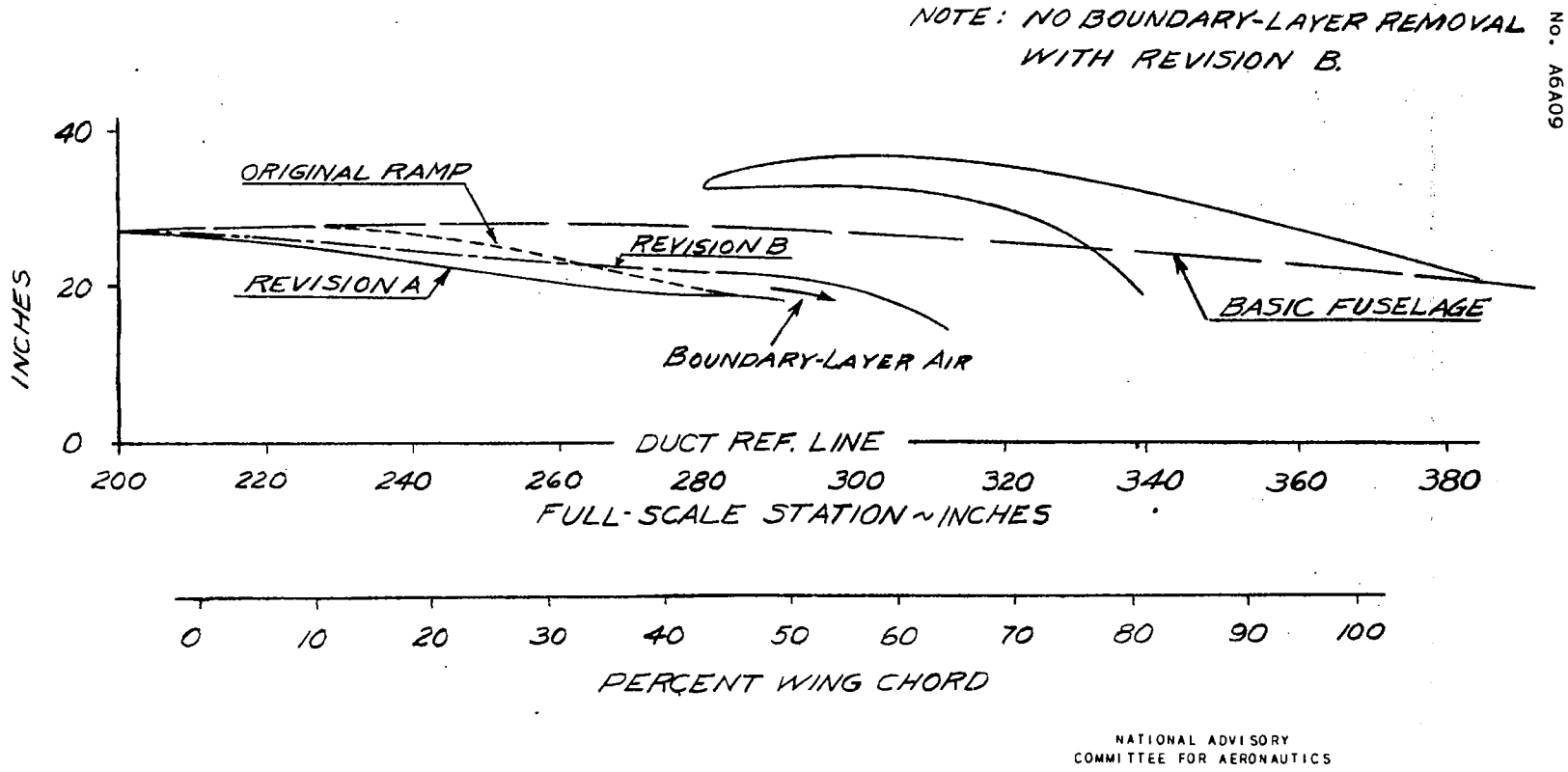

FIGURE 10.- RAMP REVISIONS OF THE DUCT SYSTEM ON THE 1/4-SCALE STUB-WING MODEL.

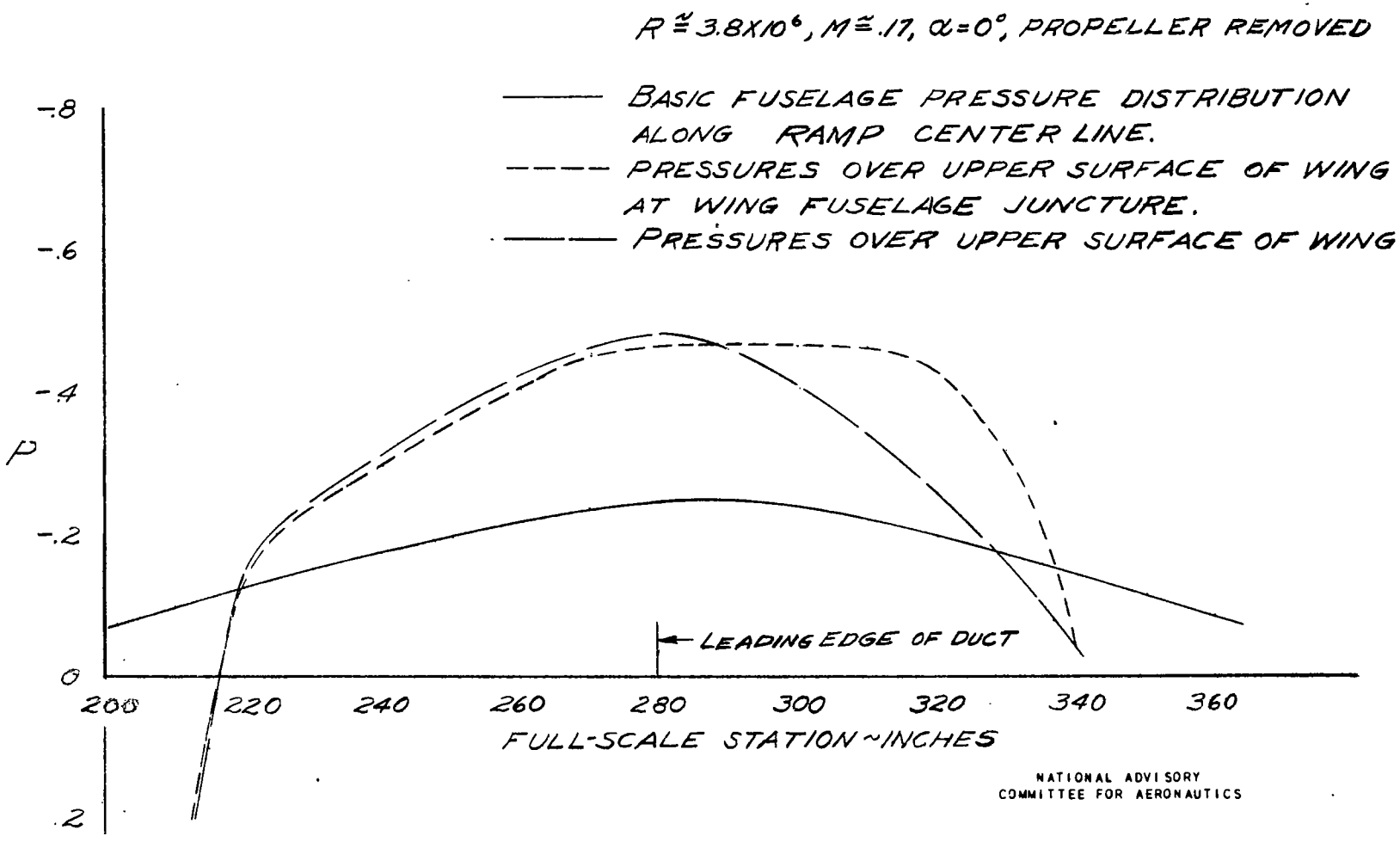

FIGURE 11.- PRESSURE DISTRIBUTION OVER THE WING AND BASIC FUSELAGE OF THE 1/4-SCALE STUB-WING MODEL.

MR No. A6A09

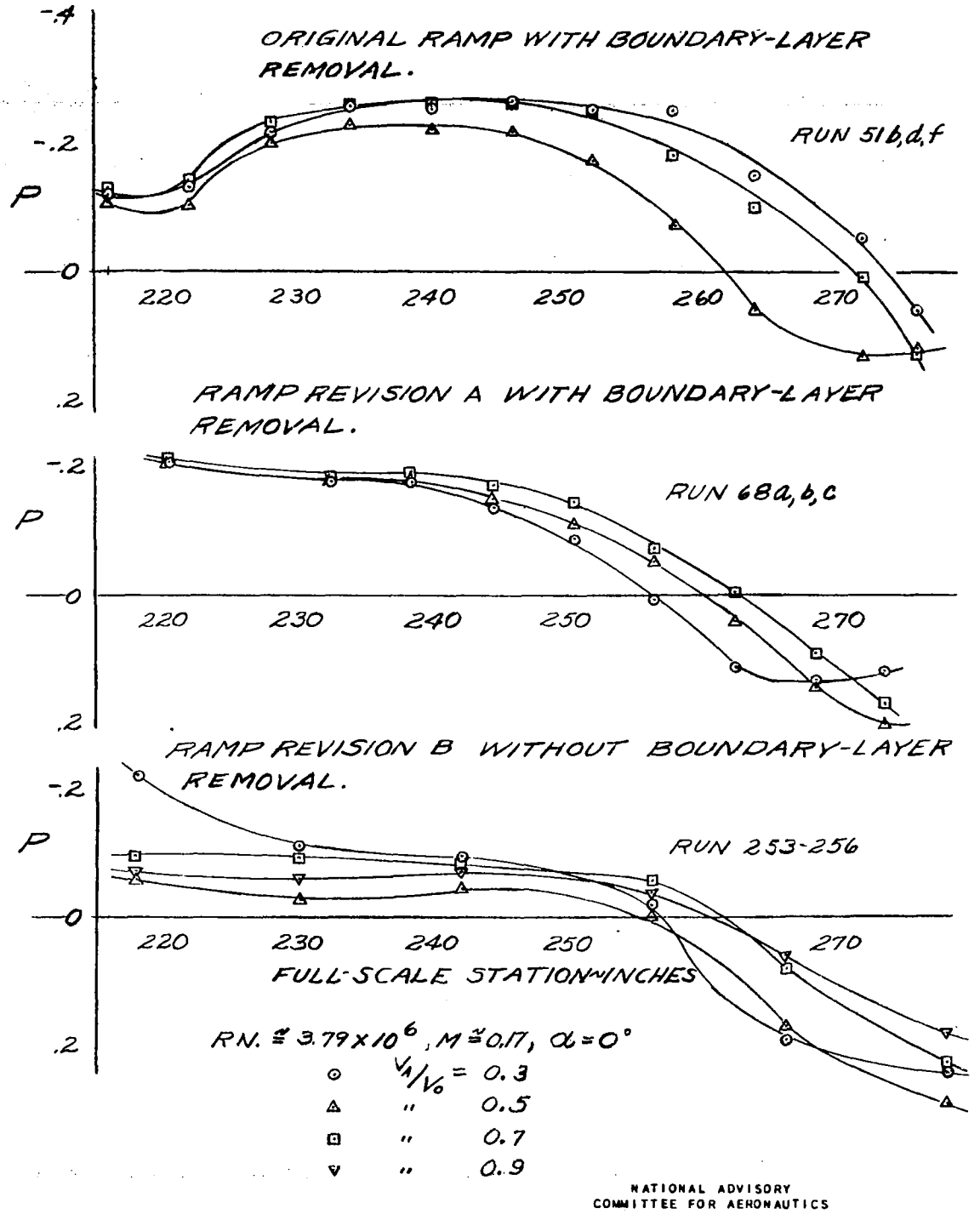

NATIONAL ADVISORY COMMITTEE FOR AERONAUTICS

FIGURE 12. -PRESSURE DISTRIBUTIONS ALONG CENTER LINES OF VARIOUS RAMPS TESTED.

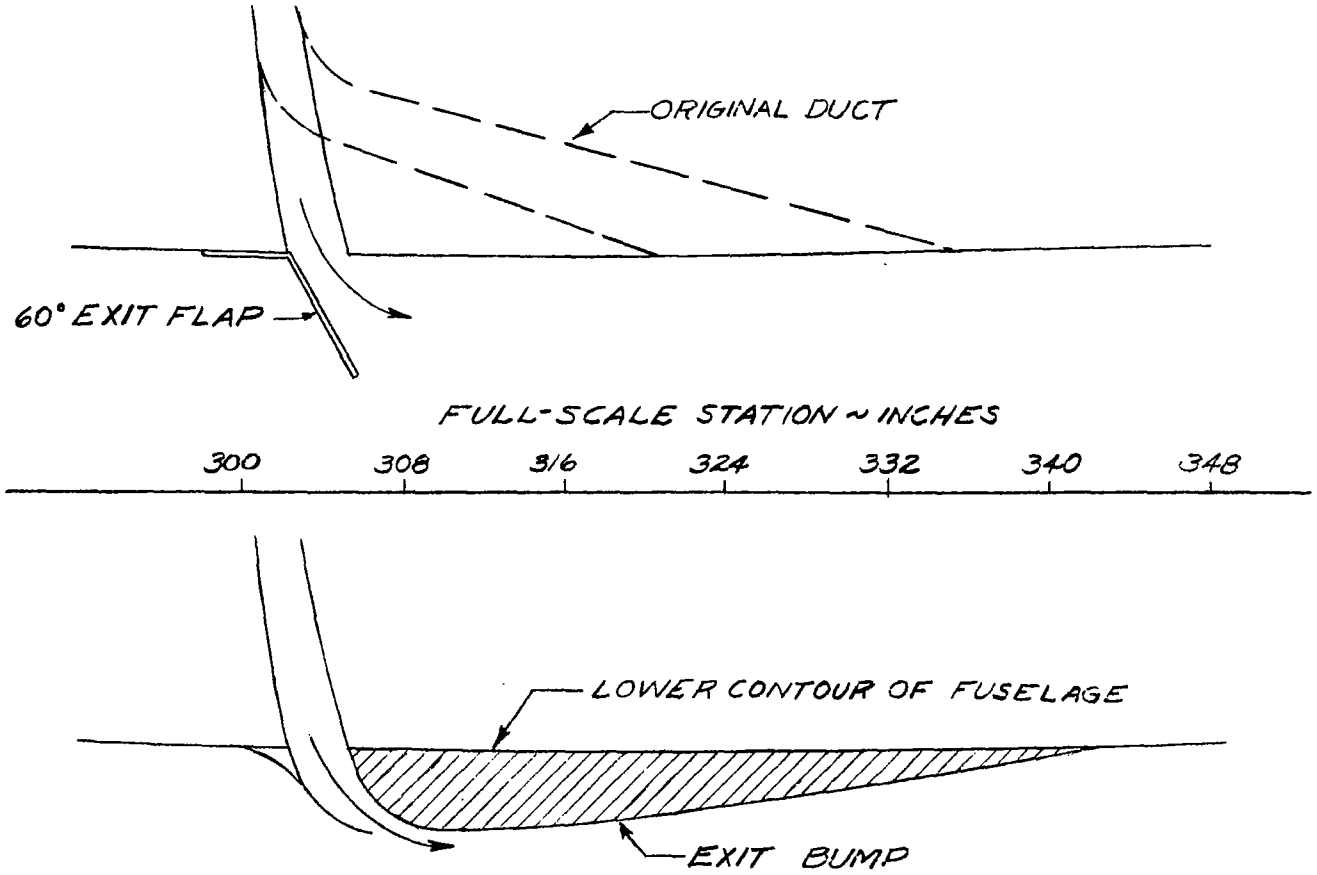

NATIONAL ADVISORY
COMMITTEE FOR AERONAUTICS

FIGURE 13. - BOUNDARY-LAYER EXIT DUCT SHOWING ORIGINAL DUCT EXIT, EXIT FLAP, AND EXIT BUMP ON THE 1/4-SCALE STUB-WING MODEL.

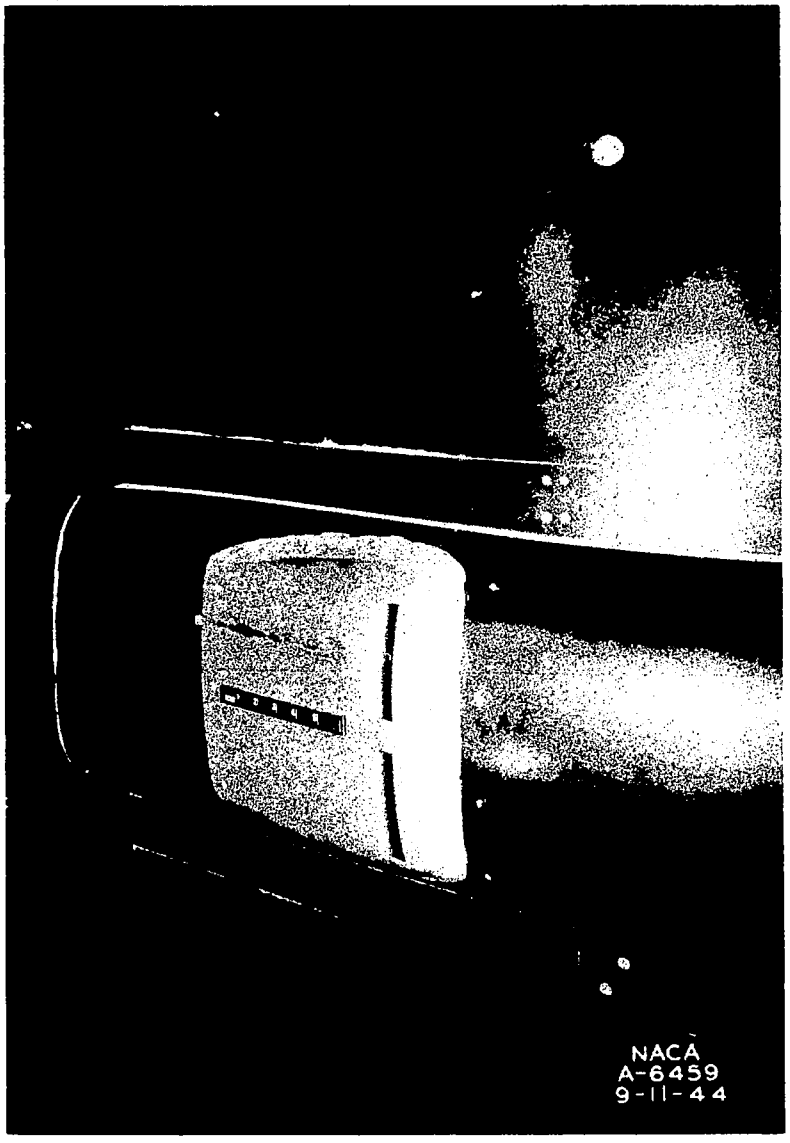

Figure 14.- Boundary-layer exit bump, 1/4-scale stub-wing model of the airplane.

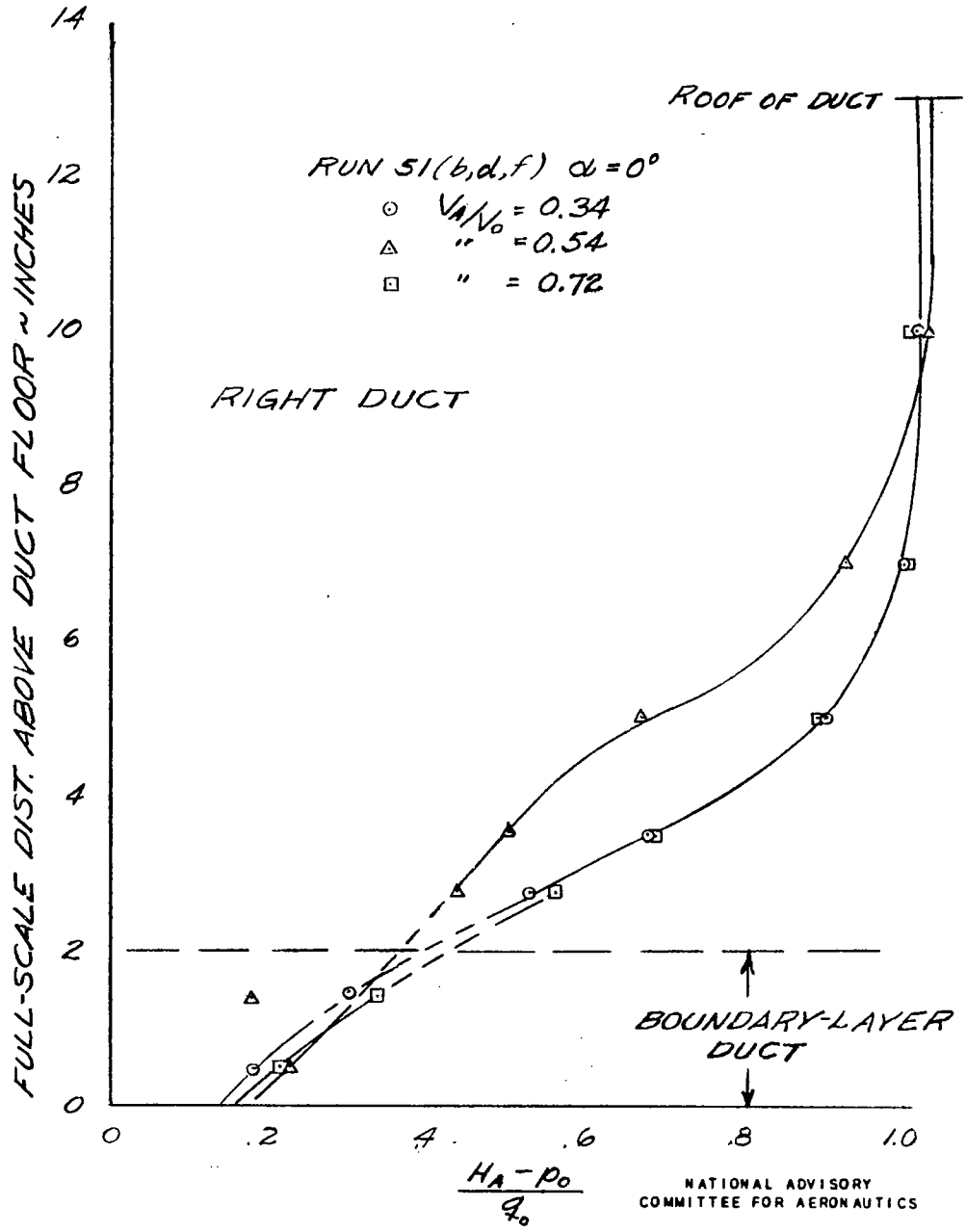

(a) ORIGINAL DUCT WITH ORIGINAL BOUNDARY-LAYER REMOVAL SYSTEM.

FIGURE 15. – TOTAL-HEAD PROFILES AT THE ENTRANCE OF THE DUCT FOR SEVERAL INLET-VELOCITY RATIOS.

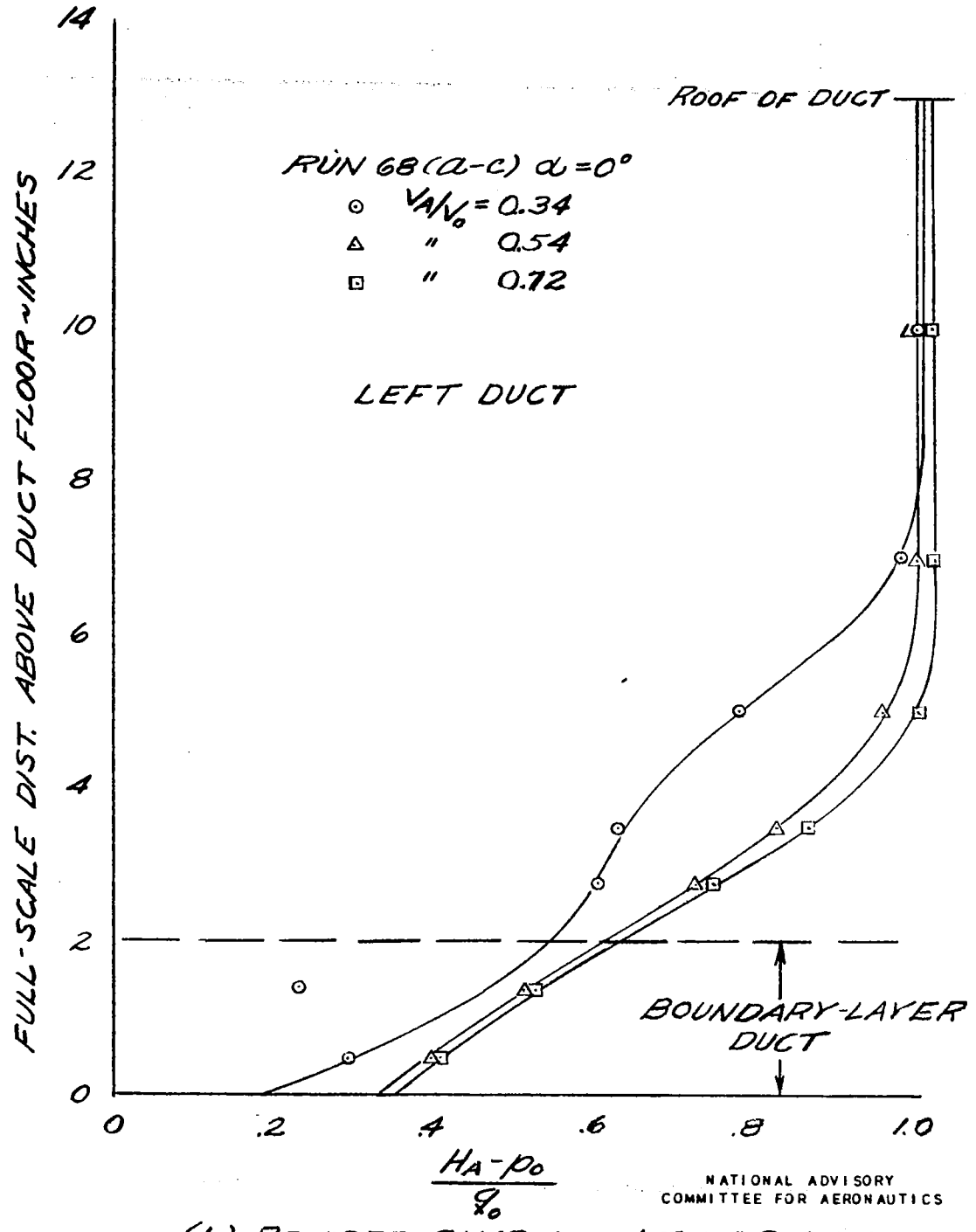

(b) REVISED RAMP A WITH ORIGINAL BOUNDARY-LAYER REMOVAL SYSTEM.

FIGURE 15. - CONTINUED.

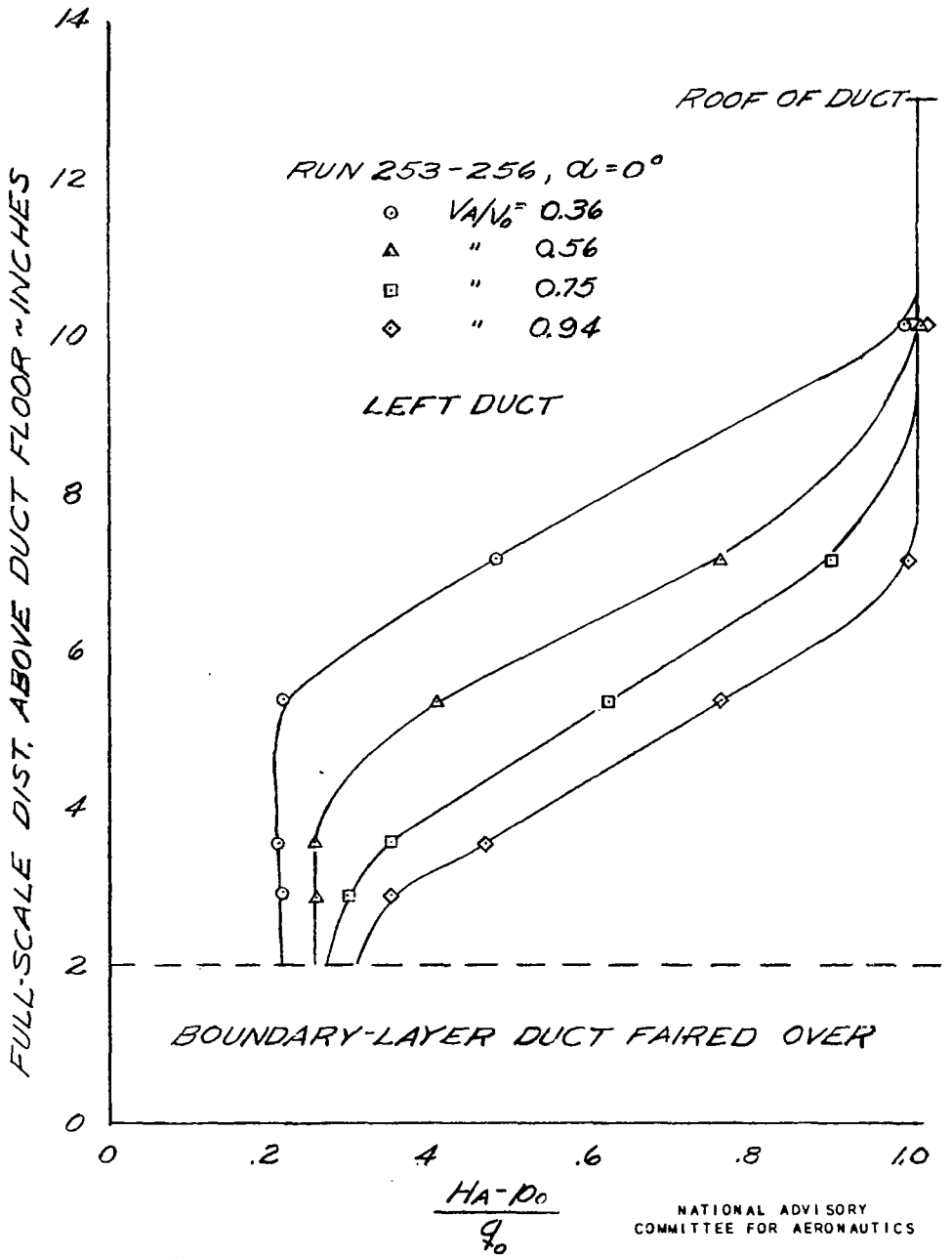

(c) REVISED RAMP B WITHOUT BOUNDARY-LAYER REMOVAL.

FIGURE 15.- CONCLUDED.

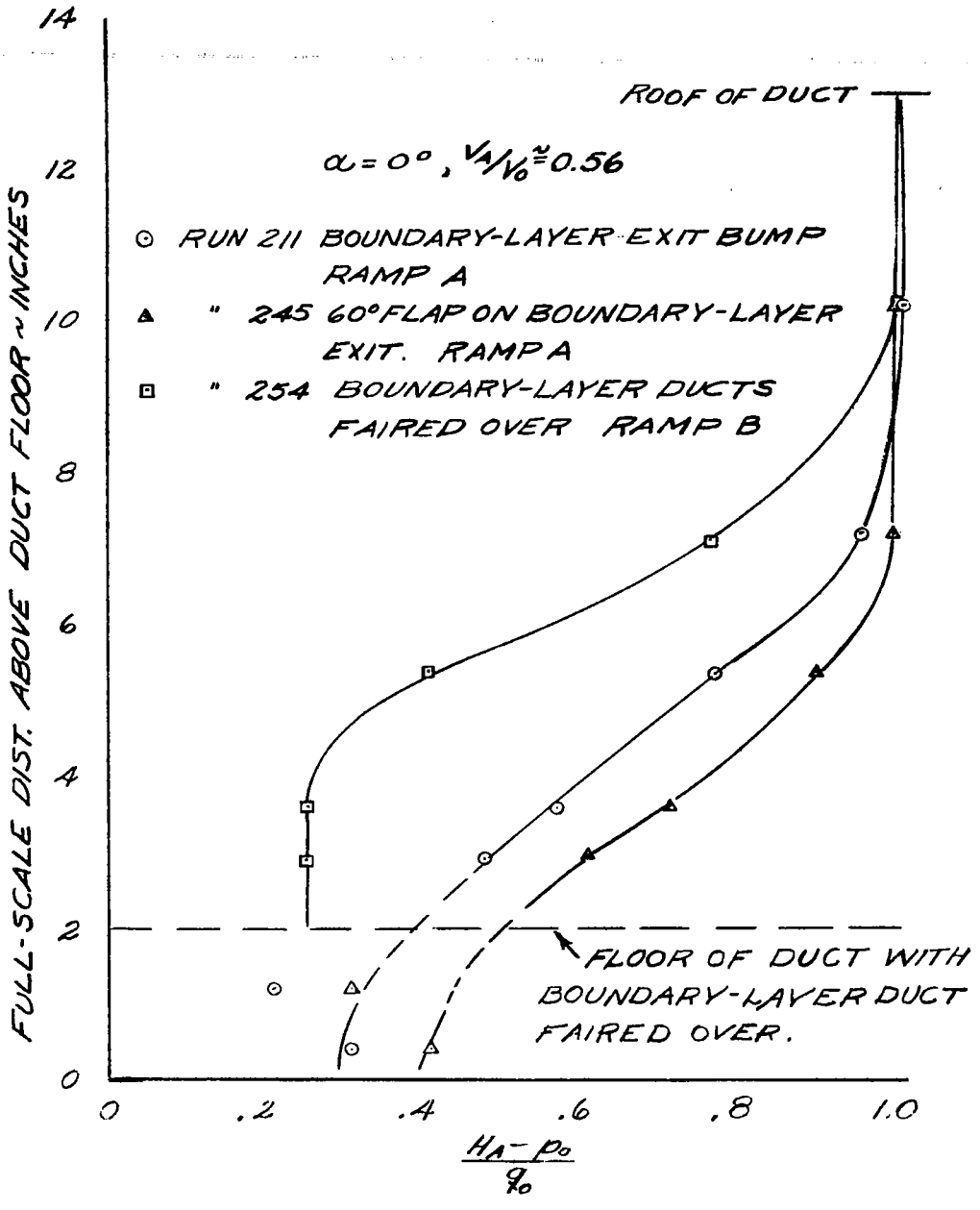

NATIONAL ADVISORY COMMITTEE FOR AERONAUTICS

(a) LEFT DUCT

FIGURE 16. - ENTRANCE PROFILES SHOWING THE EFFECT OF BOUNDARY-LAYER REMOVAL.

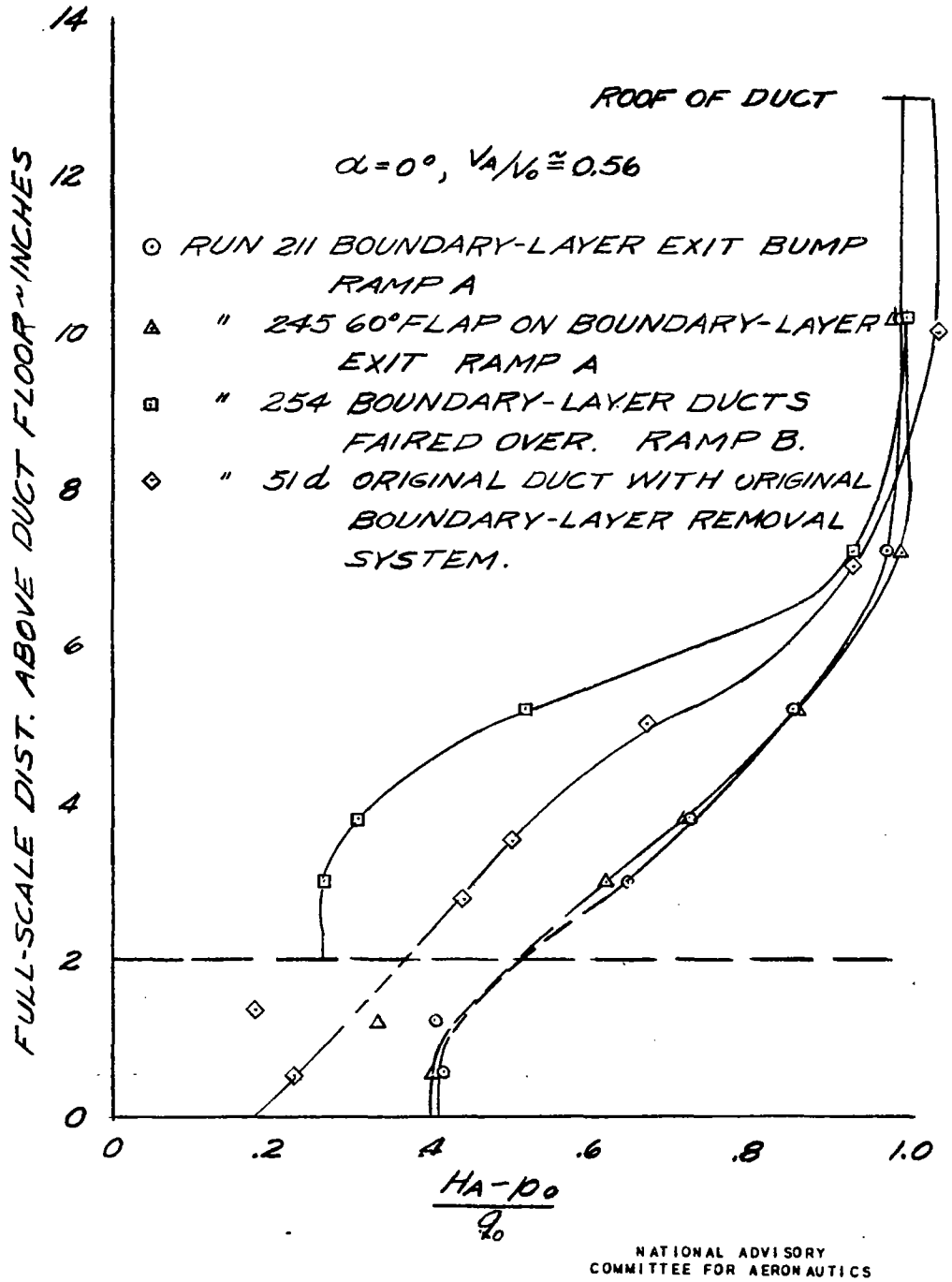

(b) RIGHT DUCT

FIGURE 16. - CONCLUDED.

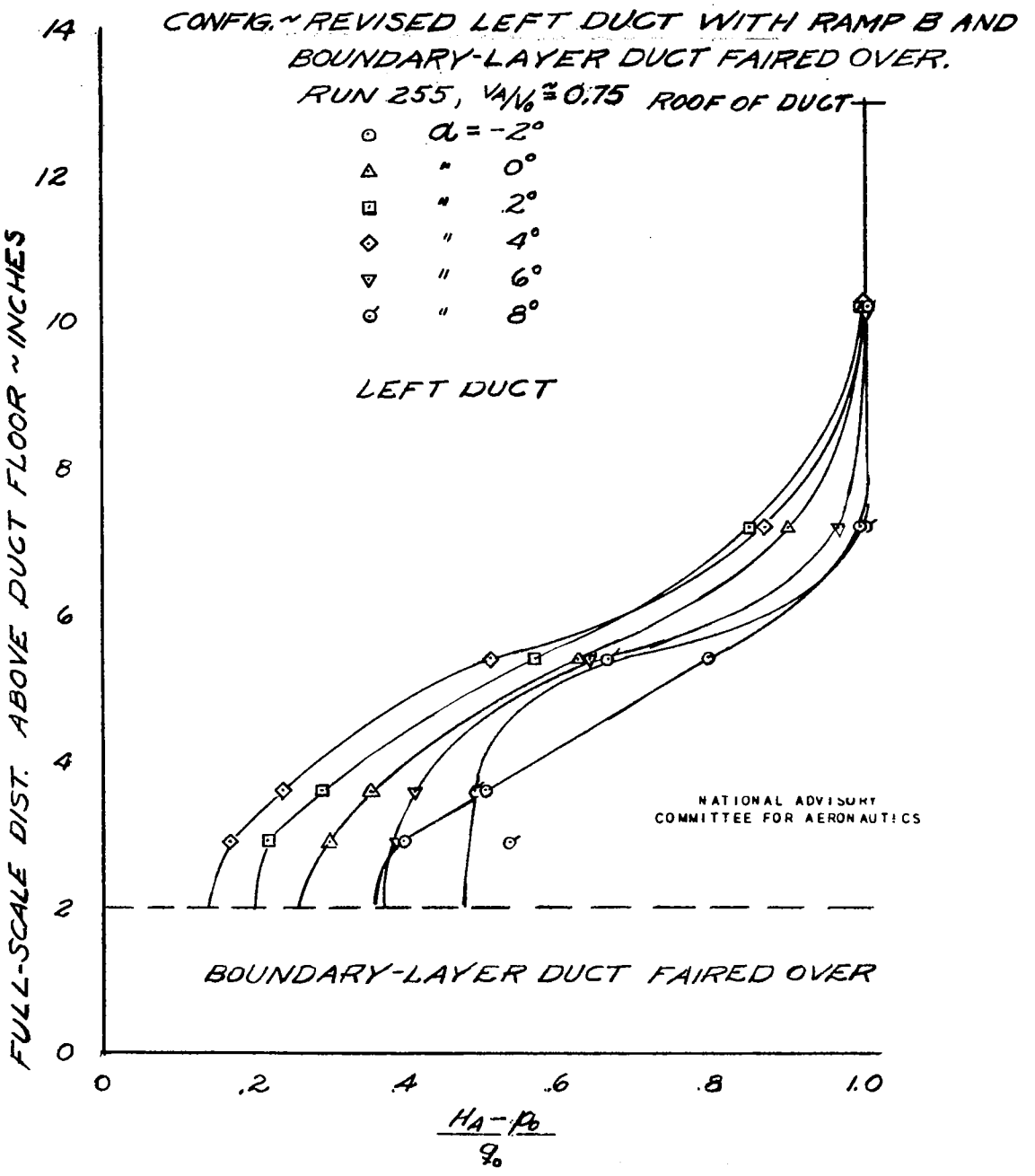

FIGURE 17. -ENTRANCE PROFILES FOR VARIOUS ANGLES OF ATTACK AT AN INLET-VELOCITY RATIO OF 0.75.

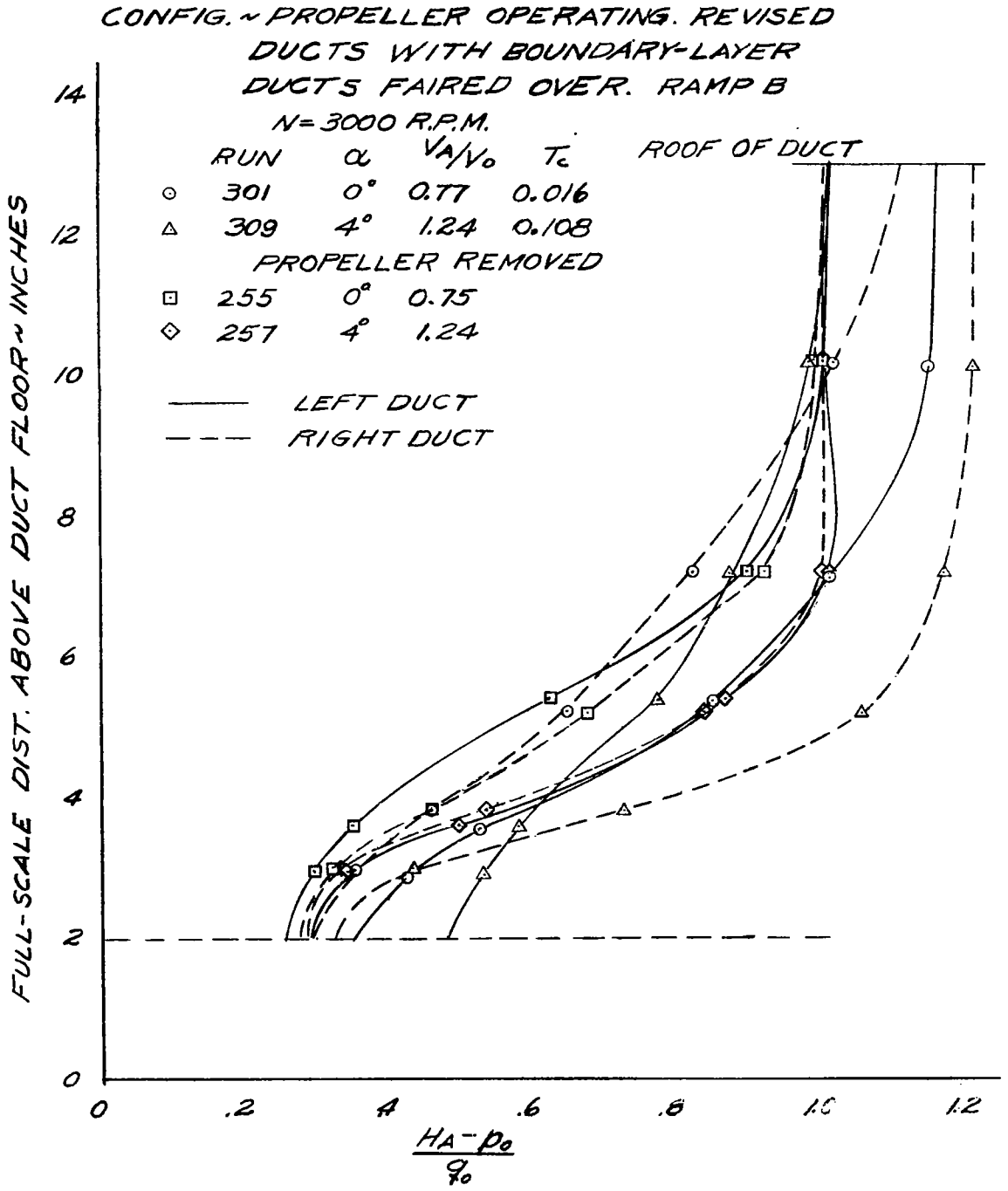

(a) $\alpha = 0$, $V_A/V_0 = 0.77$, $T_c = 0.016$
$\alpha = 4°$, $V_A/V_0 = 1.24$, $T_c = 0.108$

FIGURE 18. - ENTRANCE PROFILES WITH POWER ON FOR THE 1/4-SCALE STUB-WING MODEL.

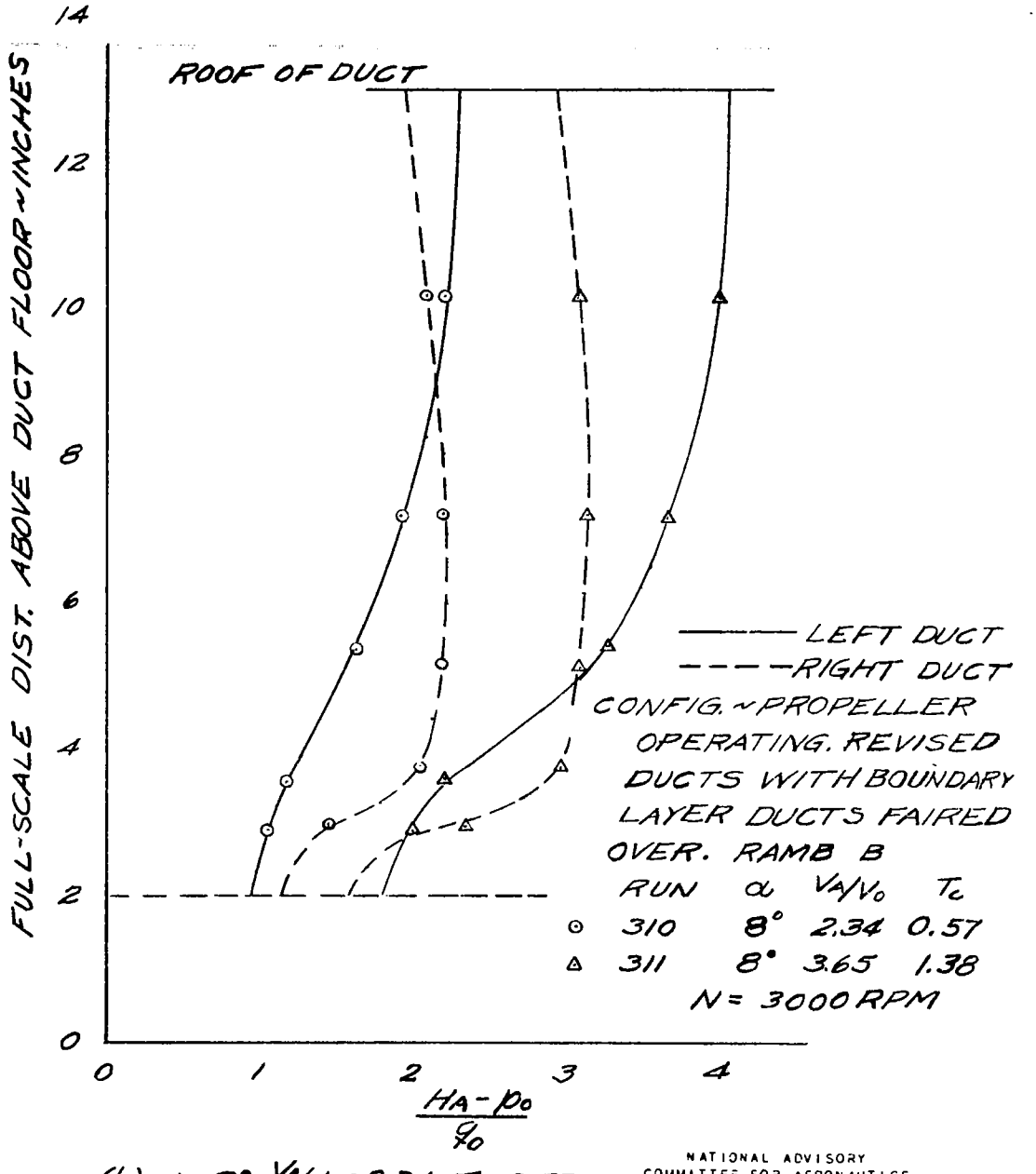

(b) $\alpha = 8°$; $V_A/V_0 = 2.34$, $T_c = 0.57$
$\alpha = 8°$ $V_A/V_0 = 3.65$, $T_c = 1.38$

FIGURE 18.- CONCLUDED.

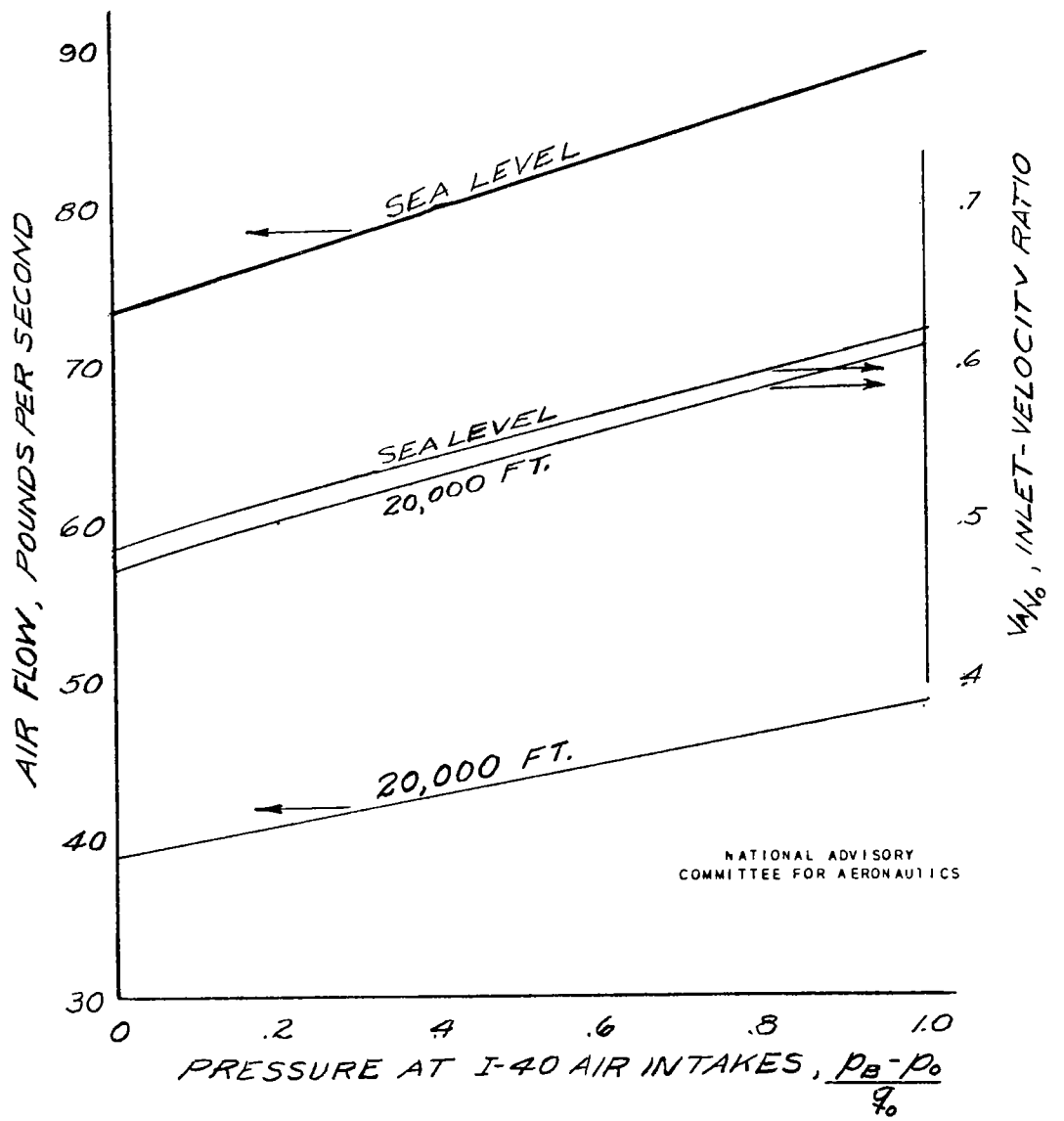

FIGURE 19.- AIR-FLOW CHARACTERISTICS AT 500 MPH FOR THE G.E. I-40 JET MOTOR.

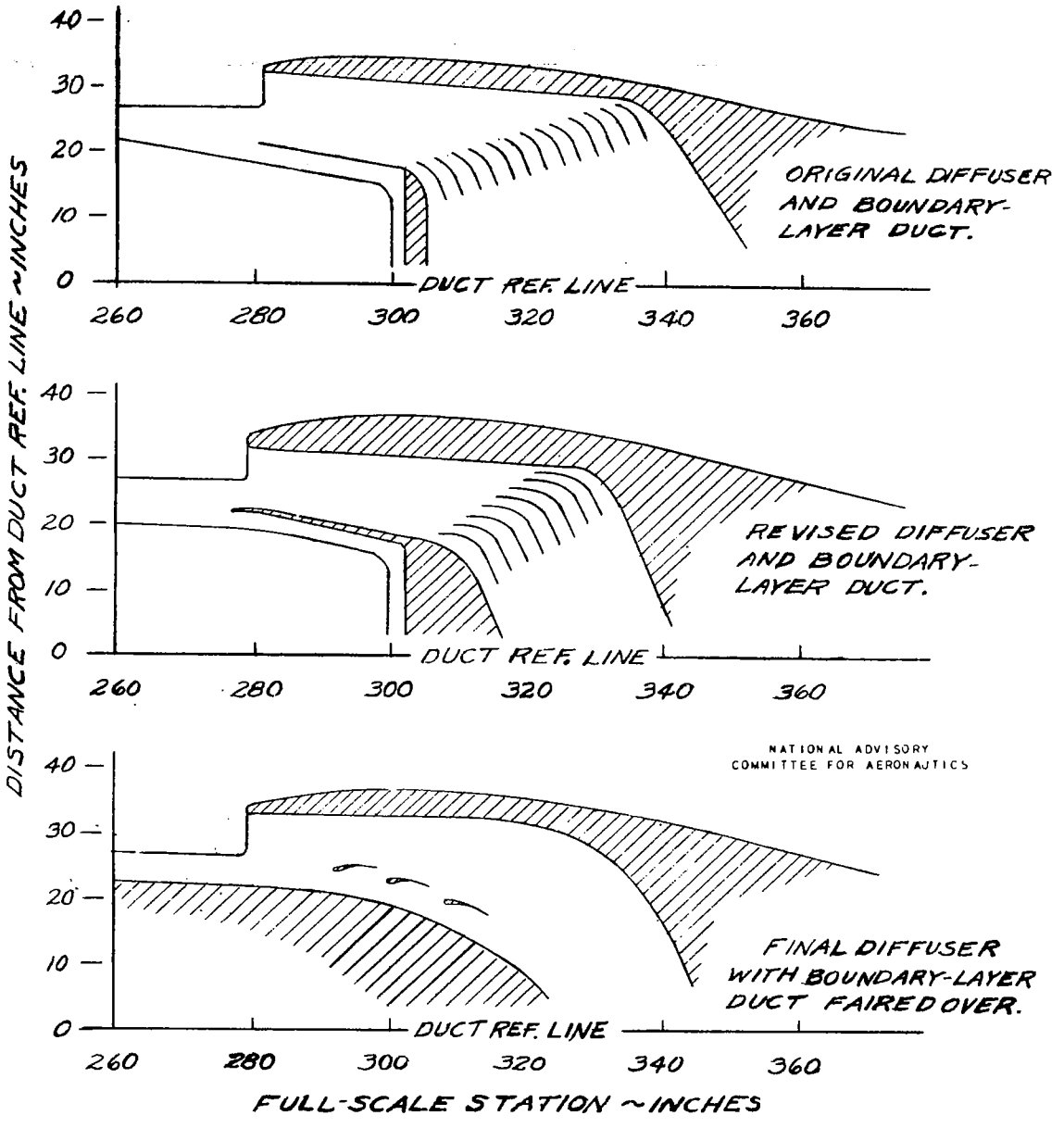

FIGURE 20. - DUCT-DIFFUSER REVISIONS ON THE ¼-SCALE STUB-WING MODEL

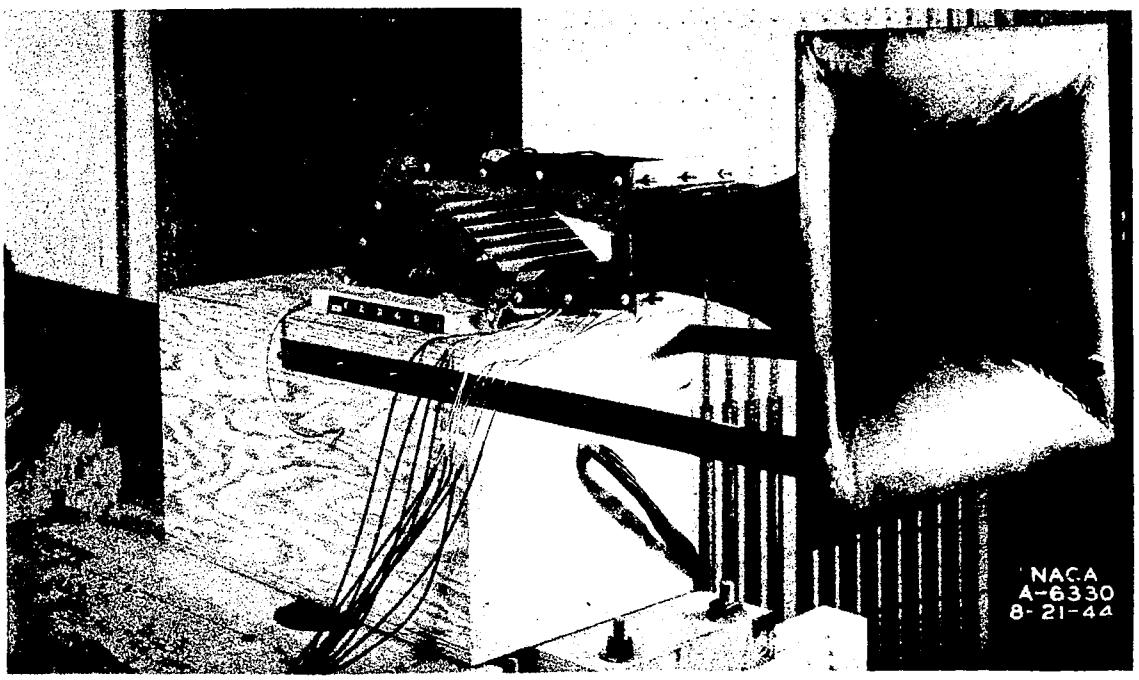

Figure 21.- Bench-test setup for testing the I-40 air-intake duct diffuser, 1/4-scale stub-wing model of the airplane.

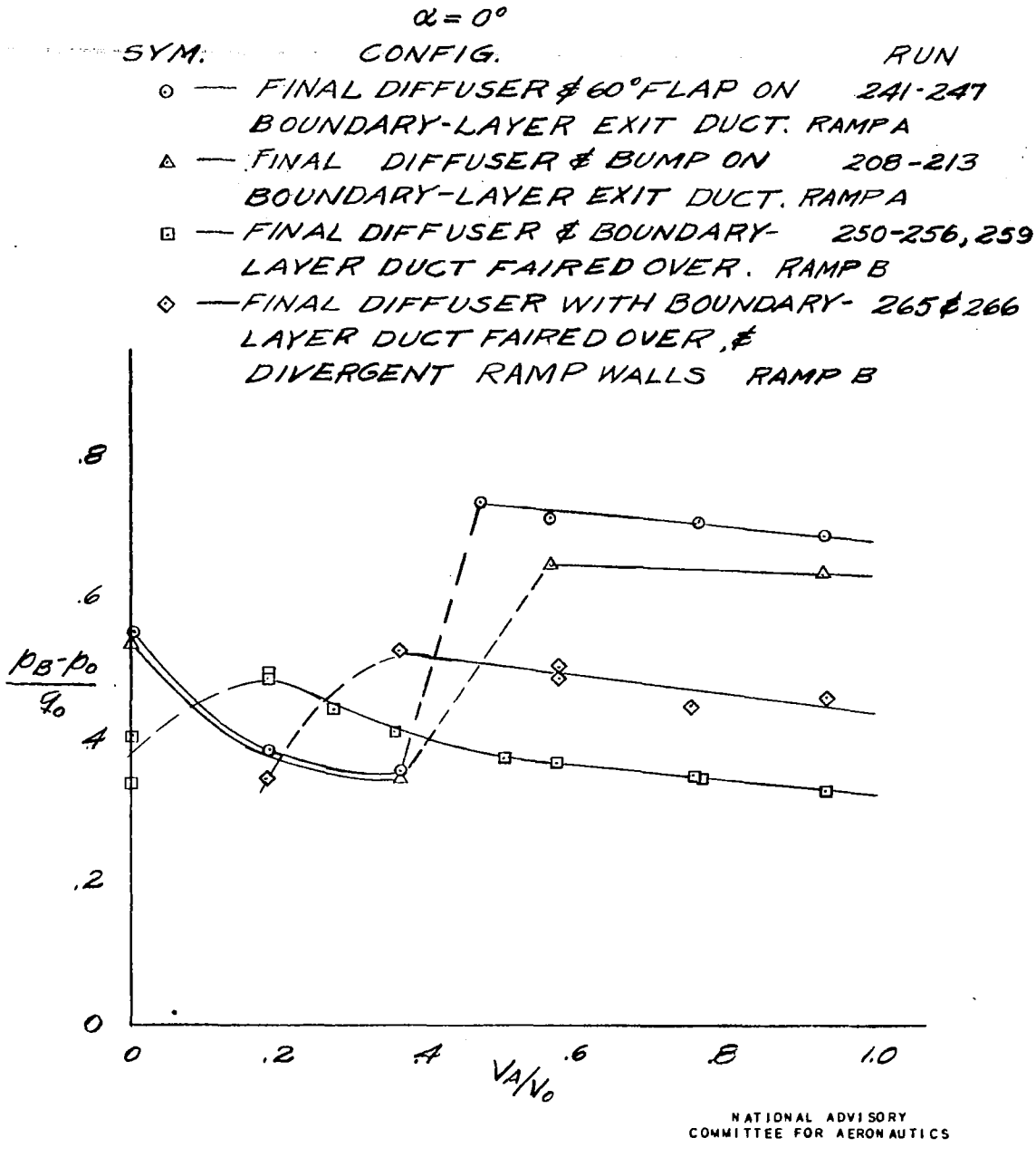

FIGURE 22. - VARIATION OF STATIC-HEAD PRESSURE RECOVERY IN THE PLENUM CHAMBER WITH INLET-VELOCITY RATIO.

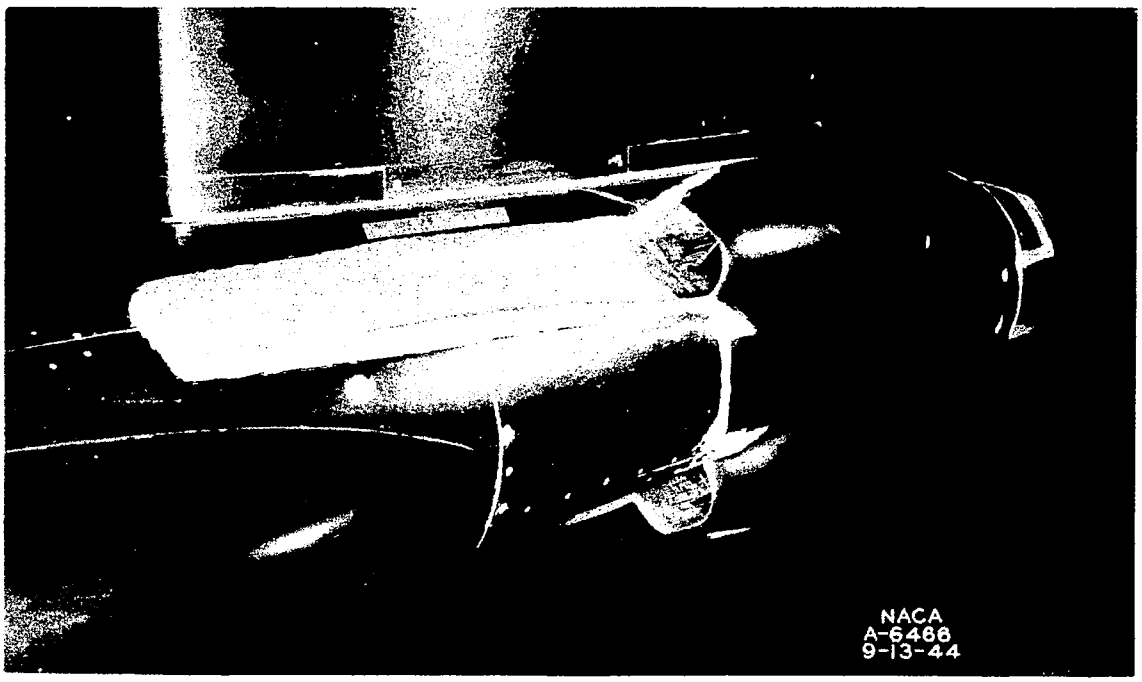

Figure 23.- Revised I-40 air-intake ducts with divergent ramp, 1/4-scale stub-wing model of the airplane.

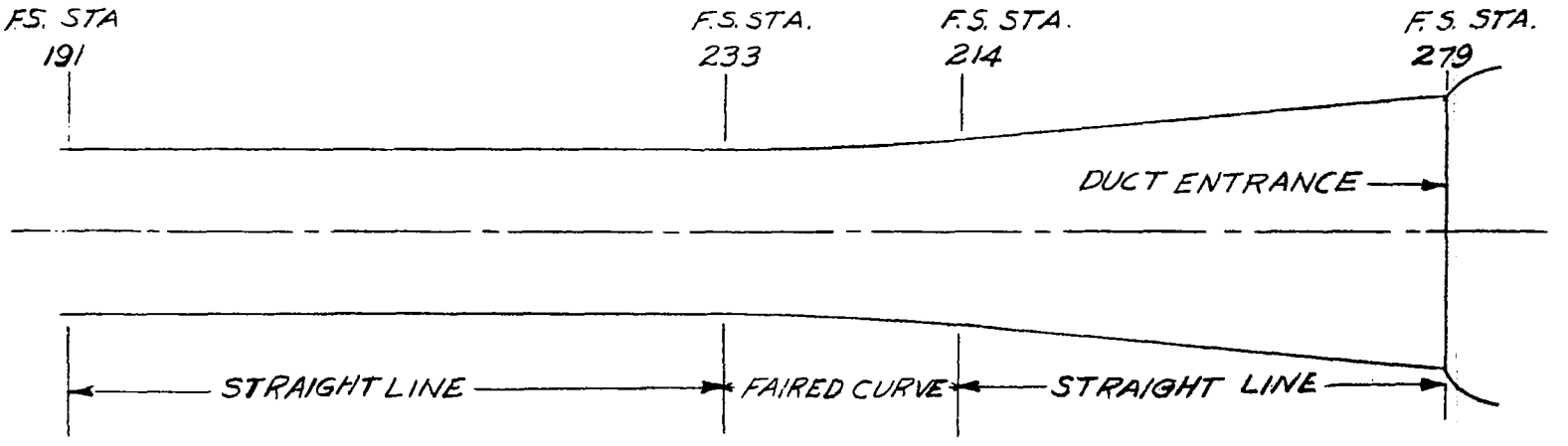

NATIONAL ADVISORY
COMMITTEE FOR AERONAUTICS

FIGURE 24 - PLAN VIEW OF THE DIVERGENT RAMP.

SYMBOL ⊙				
RUN	α°	q_o	V_A/V_o	T_c
300	0	34.4	0.57	0.021
301	2	34.4	0.76	0.020
302	2	34.5	0.93	0.022
309	4	25.0	1.24	0.110
310	8	8.7	2.34	0.570
311	8	4.0	3.65	1.380

SYMBOL △				
RUN	α°	q_o	V_A/V_o	T_c
279	0	34.4	0.57	0.015
280	2	34.2	0.75	0.014
281	2	34.2	0.95	0.016
288	4	25.0	1.23	0.100
289	8	8.7	2.33	0.550
290	8	3.8	3.84	1.510

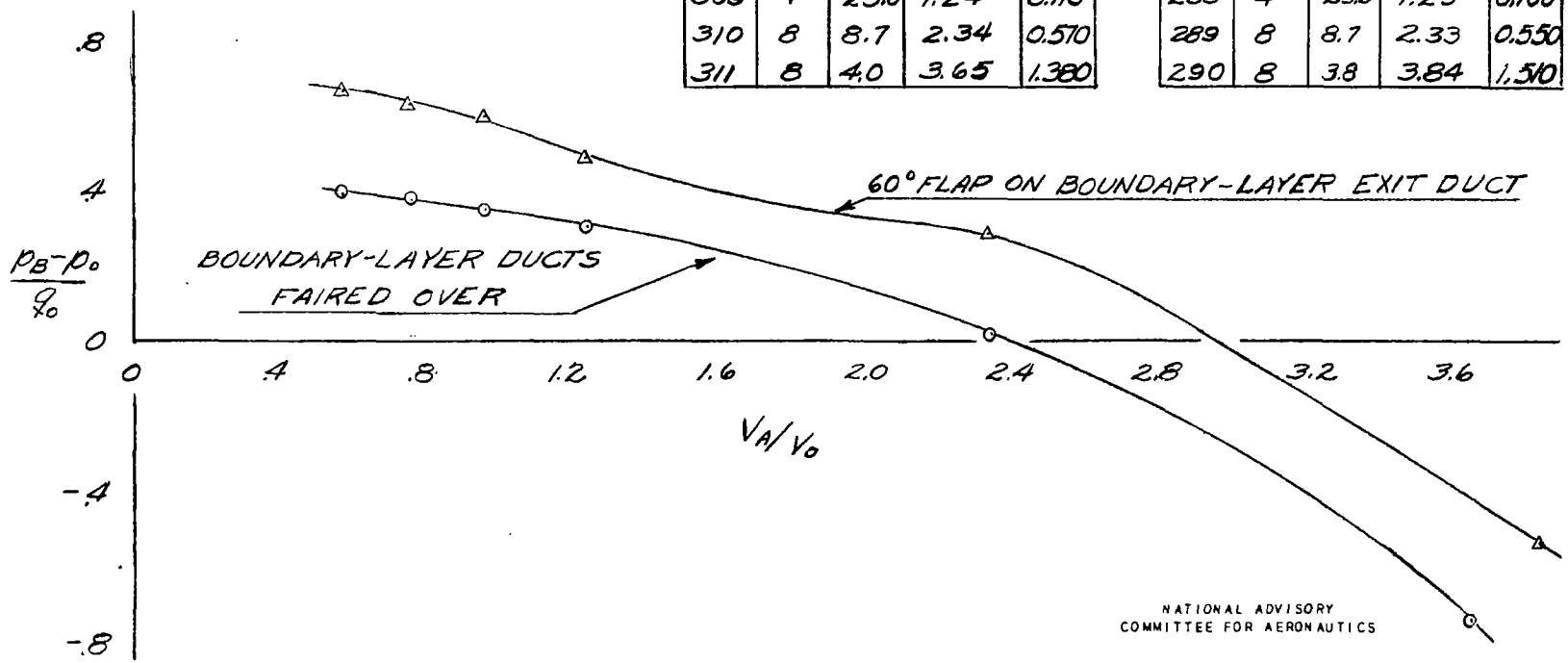

FIGURE 25. - VARIATION OF PRESSURE RECOVERY IN THE PLENUM CHAMBER WITH INLET-VELOCITY RATIO, POWER ON.

MR No. A6A09

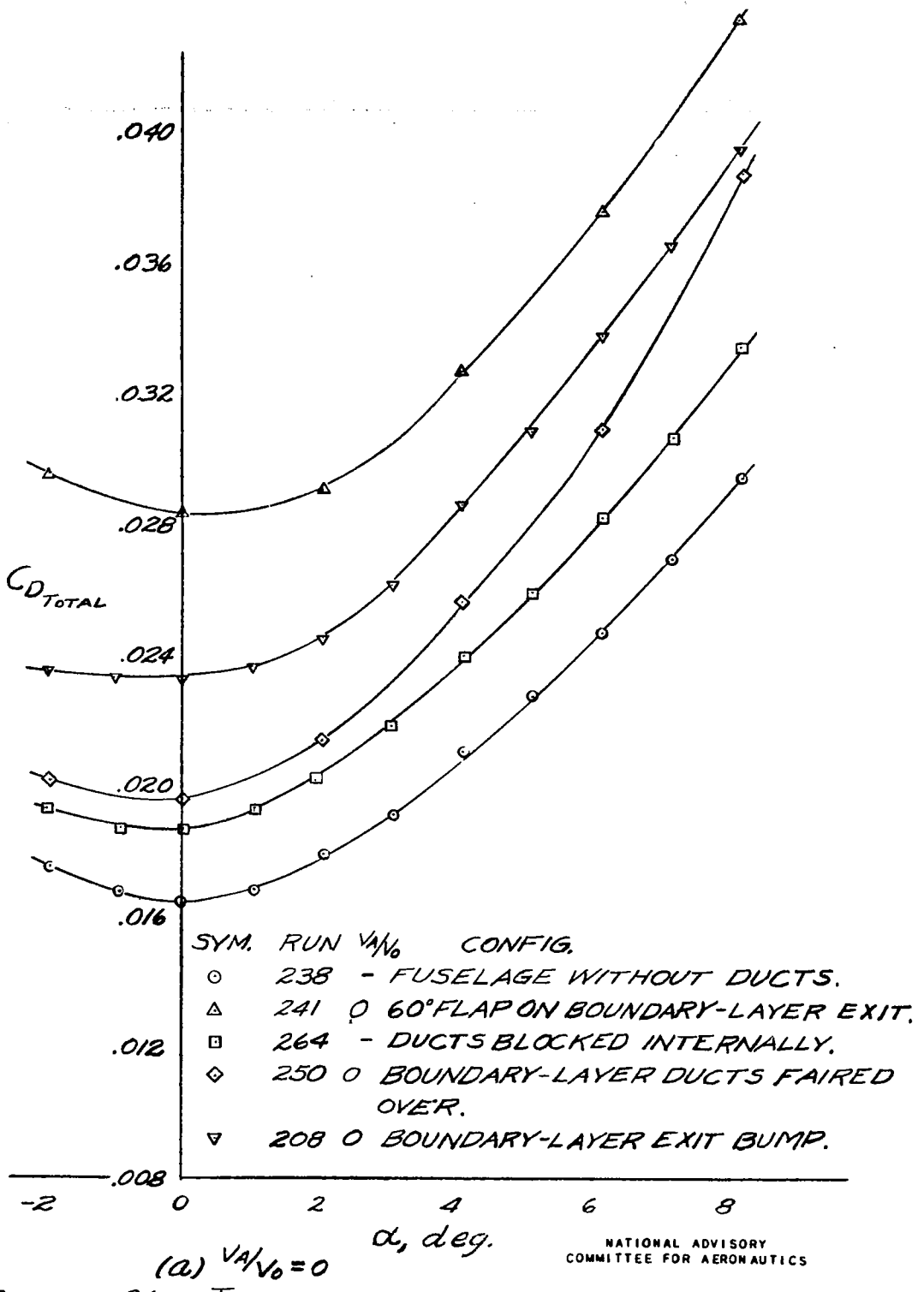

(a) $V_A/V_0 = 0$

FIGURE 26.- TOTAL DRAG OF VARIOUS CONFIGURATIONS FOR THE 1/4-SCALE STUB-WING MODEL.

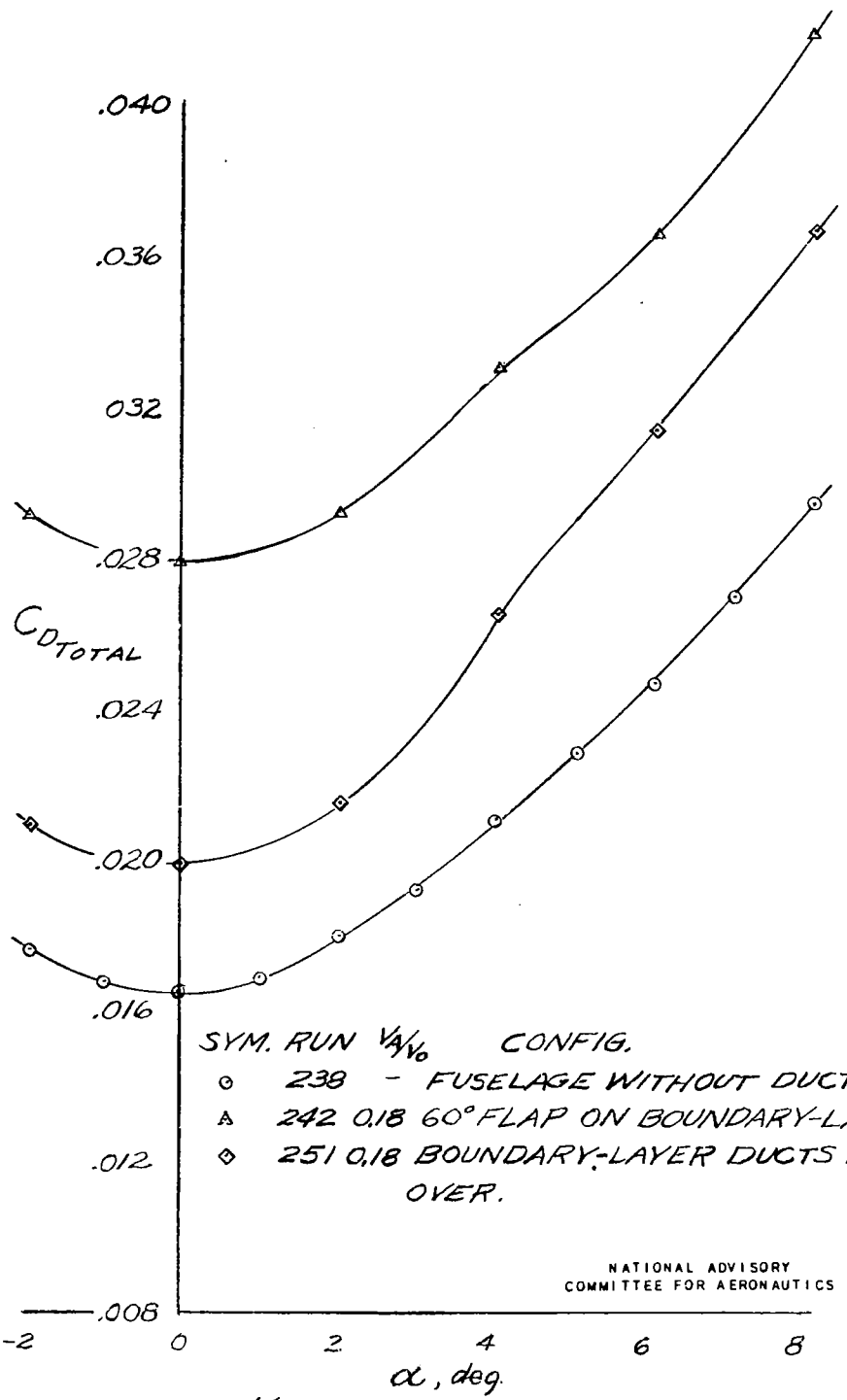

(b) $V_A/V_0 = 0.18$

FIGURE 26. - CONTINUED.

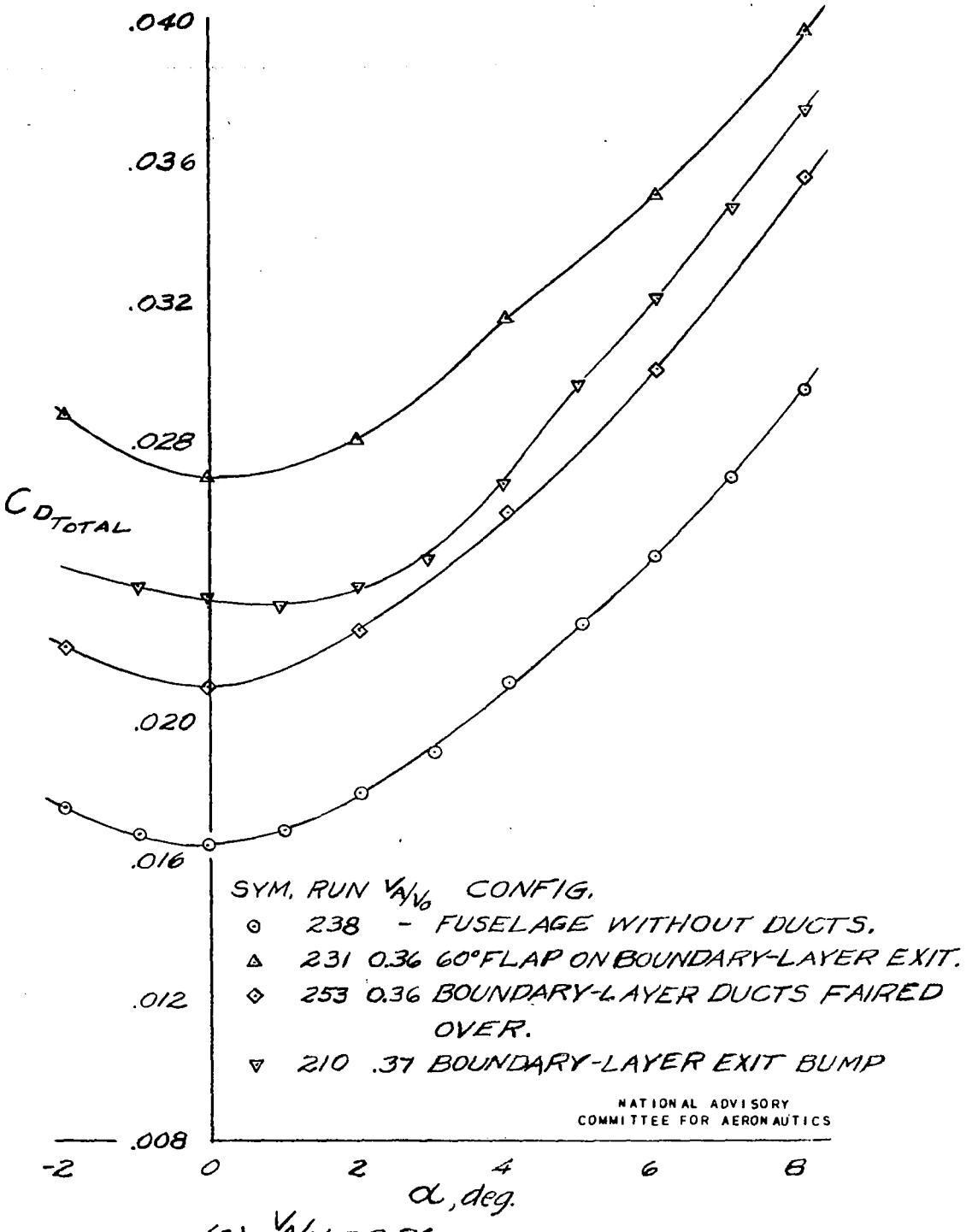

(c) $V_A/V_0 = 0.36$

FIGURE 26. - CONTINUED.

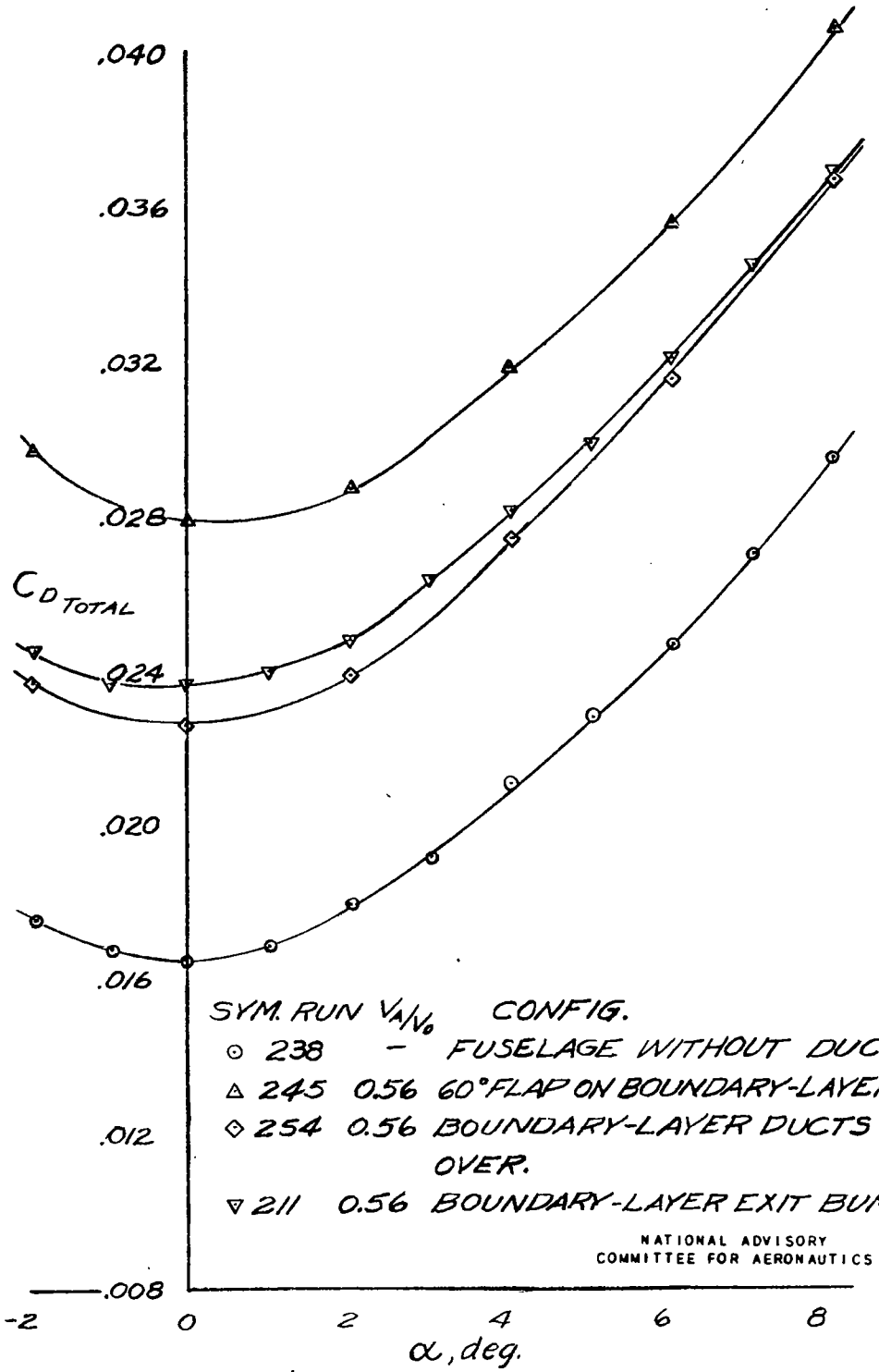

(d) $V_A/V_0 = 0.56$

FIGURE 26.- CONTINUED.

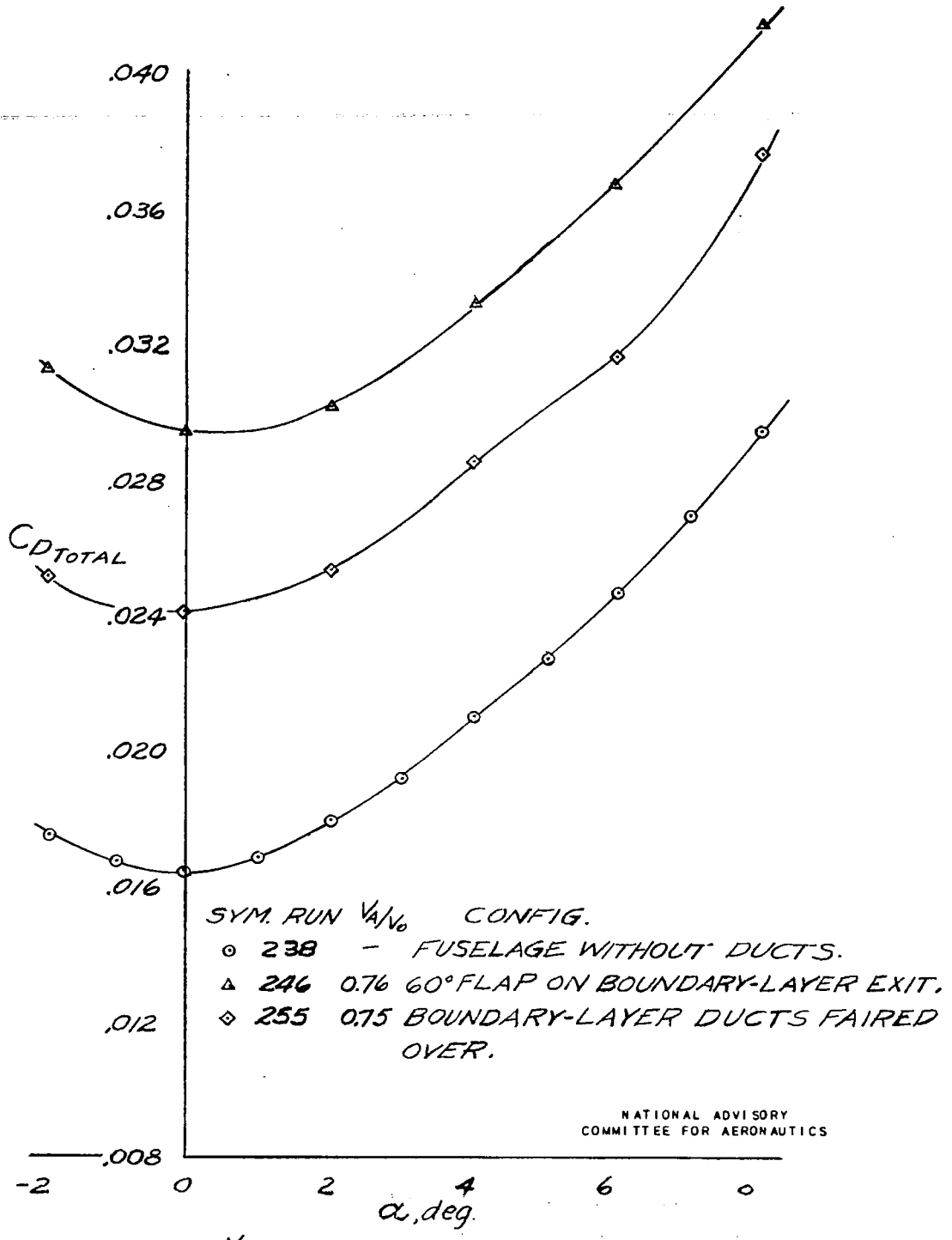

(e) $V_A/V_0 = 0.75$

FIGURE 26.- CONTINUED.

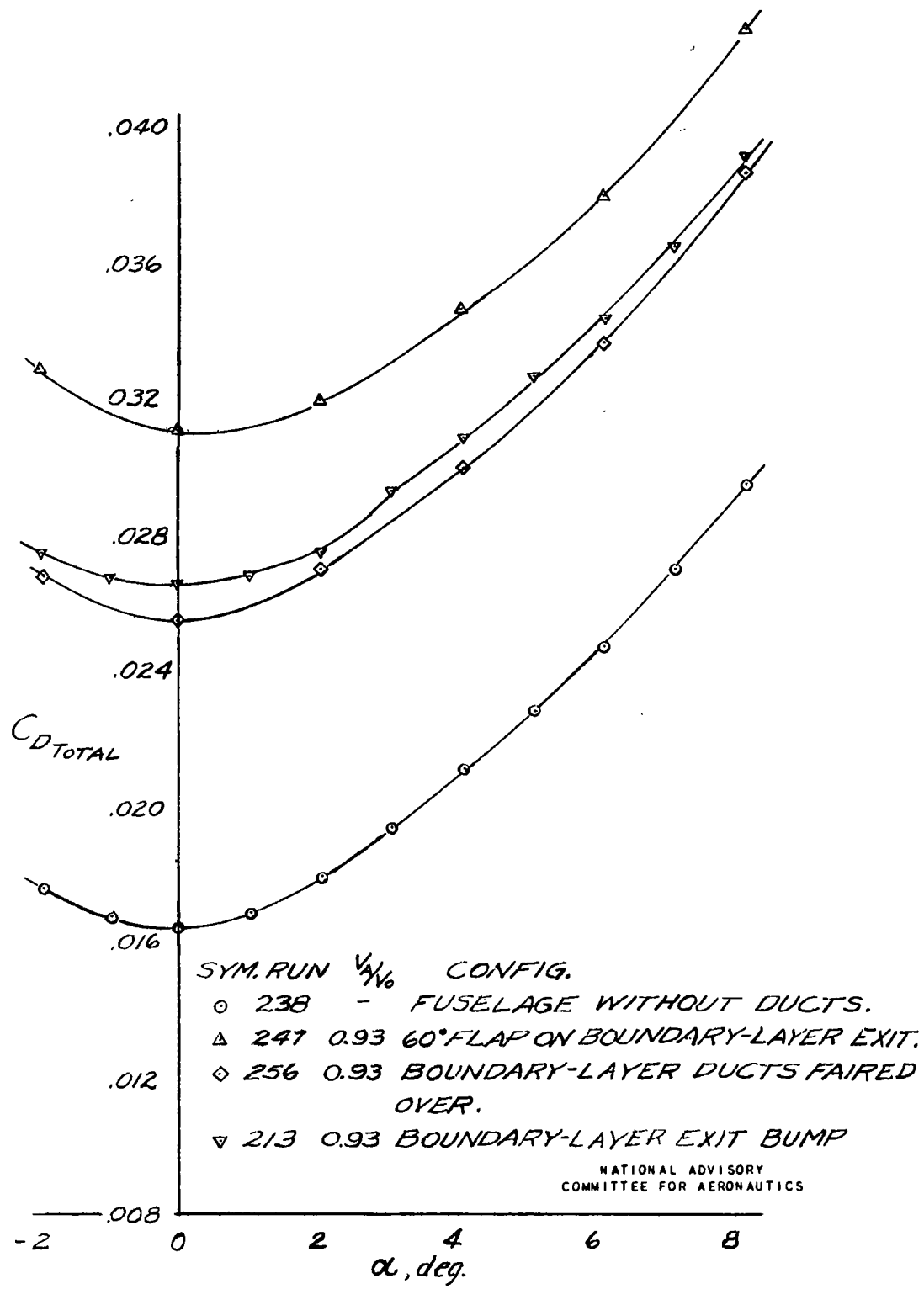

(f) $V_A/V_0 = 0.93$

FIGURE 26. - CONTINUED.

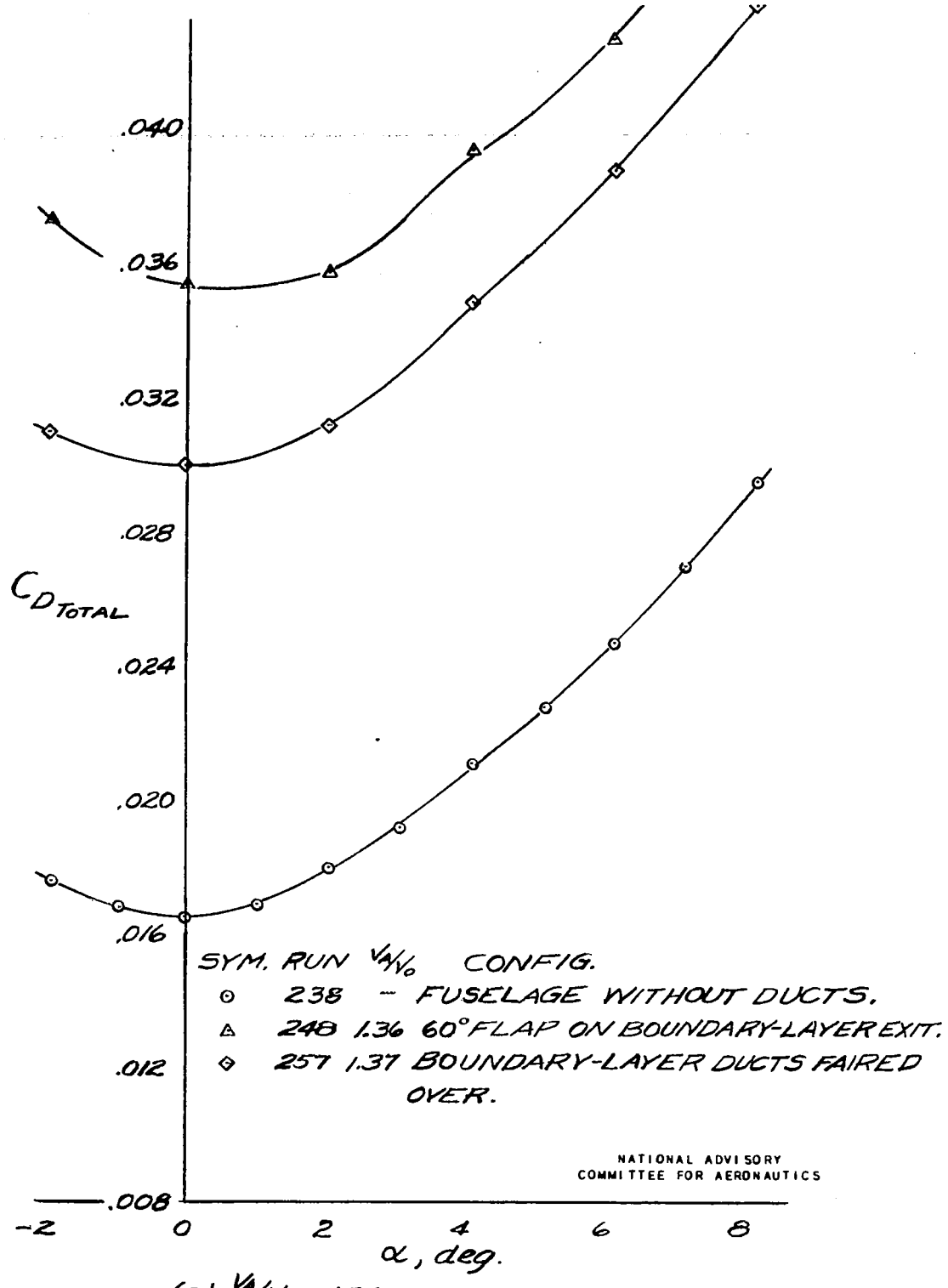

(g) $V_A/V_0 = 1.36$

FIGURE 26.– CONCLUDED.

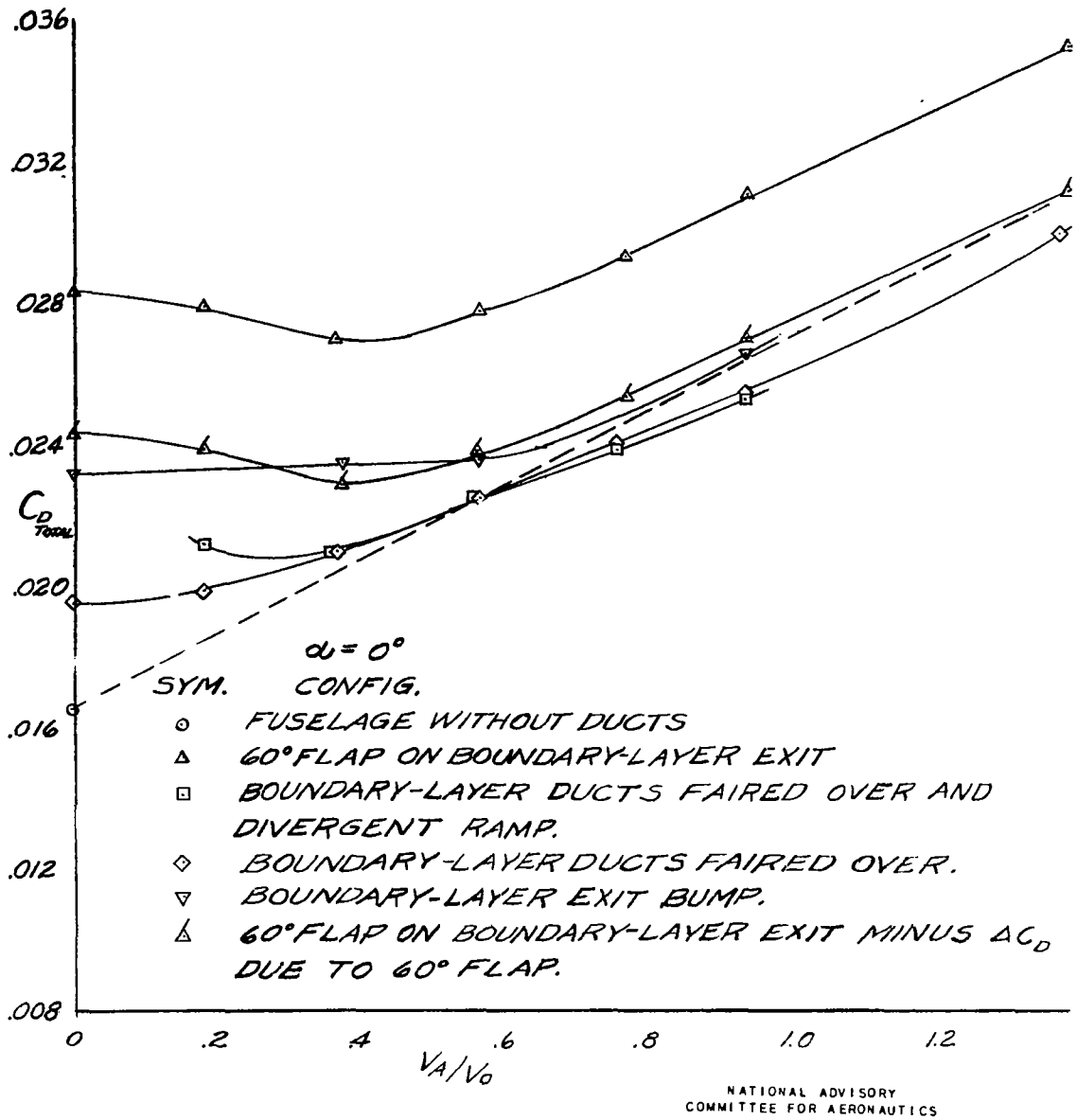

FIGURE 27. - TOTAL DRAG VS. INLET-VELOCITY RATIO FOR THE SEVERAL CONFIGURATIONS TESTED.

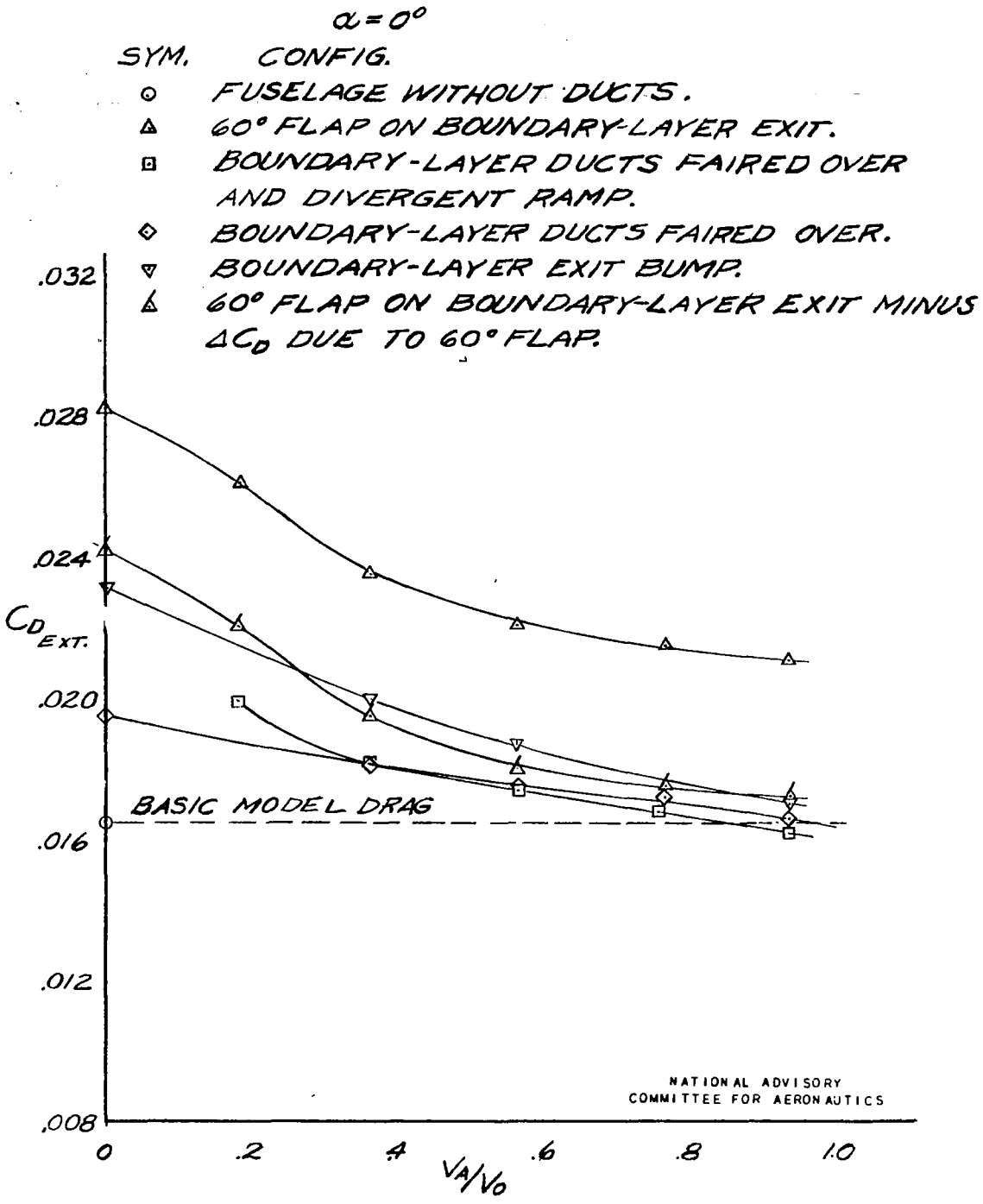

FIGURE 28.- EXTERNAL DRAG VS. INLET-VELOCITY RATIO FOR THE SEVERAL CONFIGURATIONS TESTED.